Detrital Constraints on the Southern Amadeus Basin – new analysis of zircon and apatite samples for detrital provenance and thermal evolution

Thesis submitted in accordance with the requirements of the University of Adelaide for an Honours Degree in Geology/Geophysics

YEE HENG WONG

November 2018

THE UNIVERSITY of ADELAIDE

DETRITAL CONSTRAINTS ON THE SOUTHERN AMADEUS BASIN: NEW ANALYSIS OF ZIRCON AND APATITE SAMPLES FOR DETRITAL PROVENANCE AND THERMAL EVOLUTION

RUNNING TITLE: PROVENANCE AND THERMAL EVOLUTION OF THE SOUTHERN AMADEUS BASIN

ABSTRACT

The Amadeus Basin is a Late Proterozoic to early Phanerozoic basin in central Australia, which records a complex sedimentation and thermal history throughout the basin. This study presents new analysis of zircon and apatite samples for detrital provenance and thermal evolution, focused in the southern Amadeus Basin (KULGERA). While the thermal history and provenance are well constrained for the north, such data for the southern region of the basin is lacking. Nineteen outcrop samples are analysed for detrital zircon U-Pb and provenance, one BR05DD01 drill-core sample is analysed for the AUPb and AFT ages. All sampled zircon formations share a similar prominent peak at ca. 1086 – 1163 Ma and a second prominent peak at ca. 1554 – 1791 Ma. However, all formations do not share similar provenance due to the major tectonic events from the Musgrave Province and Arunta Region, influencing sedimentation and architecture in the Amadeus Basin. Two age peaks derived in the AFT plot, 114 ± 11 Ma and 223 ± 13 Ma age populations suggesting an extensive thermal history in the apatite partial annealing zone. Due to the insufficient number of analysed apatite grains, this hinders the identification of age populations and more detailed age calculations. More data would be required for the apatite analysis in order to conclude a specified age population and age calculation.

KEYWORDS

Provenance, Thermal Evolution, Detrital Zircon, Apatite, Amadeus Basin, Musgrave Province, Arunta Region

TABLE OF CONTENTS

LIST OF FIGURES AND TABLES

[1] INTRODUCTION

The Amadeus Basin, located mostly in the southern part of Northern Territory and extending ~150 km to the west in Western Australia, is an intracratonic basin covering a vast surface area of 170,000 km^2 (Figure 1). The northern margin of the basin was tectonically modified during the ~450 – 300 Ma Alice Springs Orogeny, while the southern margin mostly documents reworking during the ~580 – 530 Ma Petermann Orogeny (Edgoose, 2013). These tectonic events induced the development of intracratonic fold-thrust belts that shaped the Amadeus Basin (Flöttmann et al., 2004). Sedimentation in the basin started during the Neoproterozoic and continued until the Early Carboniferous (Edgoose, 2013).

More than 30 exploratory wells have been drilled in the Amadeus Basin since 1958 until present. Two significant hydrocarbon discoveries in the Amadeus Basin are the Palm Valley Gas Field and the Mereenie Oil and Gas Field situated in the northern region (Roe, 1991). Since these discoveries, the northern and eastern region of the basin have been widely explored and scientifically studied mainly focusing on the Ordovician petroleum system (Korsch and Kennard, 1991). Comparably, the southern region of the basin is underexplored, although in recent years extensive structural, geothermal and lithological studies have been conducted (e.g. EP 125 by Santos 2014).

Peter Tingate (1991) conducted a low-temperature thermochronological study using Apatite Fission Track (AFT) on 28 drill core and outcrop samples of the Pacoota and Stairway Sandstone (Early Ordovician) in the northern part of the Amadeus Basin (Figure 2). In this study, the majority of AFT ages span between ca. 250 and 650 Ma with the younger fission tracks reflecting total or near total annealing tracks from burial related with Alice Springs Orogeny. Tingate (1991) concluded from his fission track

data that the inferred maximum temperature, between 70 and 110°C was experienced at ~360 Ma as a result of a burial process. Subsequent protracted cooling was modelled to continue until present-day. The onset of the protracted cooling was, therefore, interpreted to be driven by uplift and erosion which has occurred since the Alice Springs Orogeny. Furthermore, Gibson *et al* (2005) studied the thermal history of the Wallara-1 well (within the southern region, Figure 1) through AFTA and vitrinite reflectance (VR) data. A saw-tooth thermal history was reconstructed in this study, suggesting the timing of maximum paleotemperature (167 – 180°C) was reached within large intervening period between the Neoproterozoic (~1100 Ma) and early Triassic (~240 Ma), followed by multiple cooling and re-heating events until present (resulting in the saw-tooth shaped thermal history). Besides this study on one well, other thermochronological data for the southern part of the basin are currently absent.

Several detrital zircon U-Pb studies have been done for samples at a number of stratigraphic levels within the Amadeus Basin (Figure 1). These studies have shown that the Heavitree Quartzite, at the base of the Amadeus successions, has prominent zircon age peaks at ~1800 – 1400 Ma, suggesting that this formation was most likely derived from the adjacent Arunta Region that is characterised by similar aged igneous and metamorphic events (Zhao et al., 1992). Upper Neoproterozoic to Lower Cambrian samples display strong zircon U-Pb age peaks at ~1050 – 1200 Ma, suggesting that these samples are likely to be derived from the Musgrave Province and orogenic zones towards to the south (Camacho et al., 2002; Buick et al., 2005). The Larapinta Group (Late Cambrian – Early Devonian) shows evidence of opening to the east and clastic material sourced from eastern Australia. The Devonian succession, which is the final phase of sedimentation is entirely terrestrial and deposited during the early phase of

Alice Springs Orogeny uplift, sourcing from the Arunta Region (Haines and Wingate, 2007). Most of the zircon U-Pb studied were done in the northern region of the Amadeus Basin and are lacking for the south.

This study aims to unravel the provenance and thermal (temperature-time) evolution of the sediments in the southern Amadeus Basin utilizing zircon and apatite U-Pb and AFT data from drill-core and outcrop samples. Detrital zircon grains are classified to be one of the most powerful tools for the provenance analysis because they are largely resistant to mechanical and chemical alteration and, therefore, mostly preserve their crystallization ages of the source regions (McLennan et al., 1993; Dickinson and Gebrels, 2009). The U-Pb age of detrital zircon grains can be obtained quickly with the use of cathodoluminescence (CL) imaging and laser ablation inductively coupled plasma mass spectrometry (LA-ICP-MS) (Gebrels, 2014). Concordia plots are used to determine if zircon has been isotopically disturbed. If zircon U-Pb ratios have not been disturbed, the spot analysis will plot on the Concordia (Howard et al., 2004). The AFT method allows to model the thermal history between ~60 – 120^{o}C (Wagner and Van den haute, 1992). If apatite samples remained below 60^{o}C, the AFT ages retain a provenance age that may correspond to the zircon and apatite U-Pb system. Conversely, if temperature rises above 60 – 120^{o}C, low temperature thermal history modelling is implemented to show the post-depositional thermal history of the samples (Reiners and Ehlers, 2005).

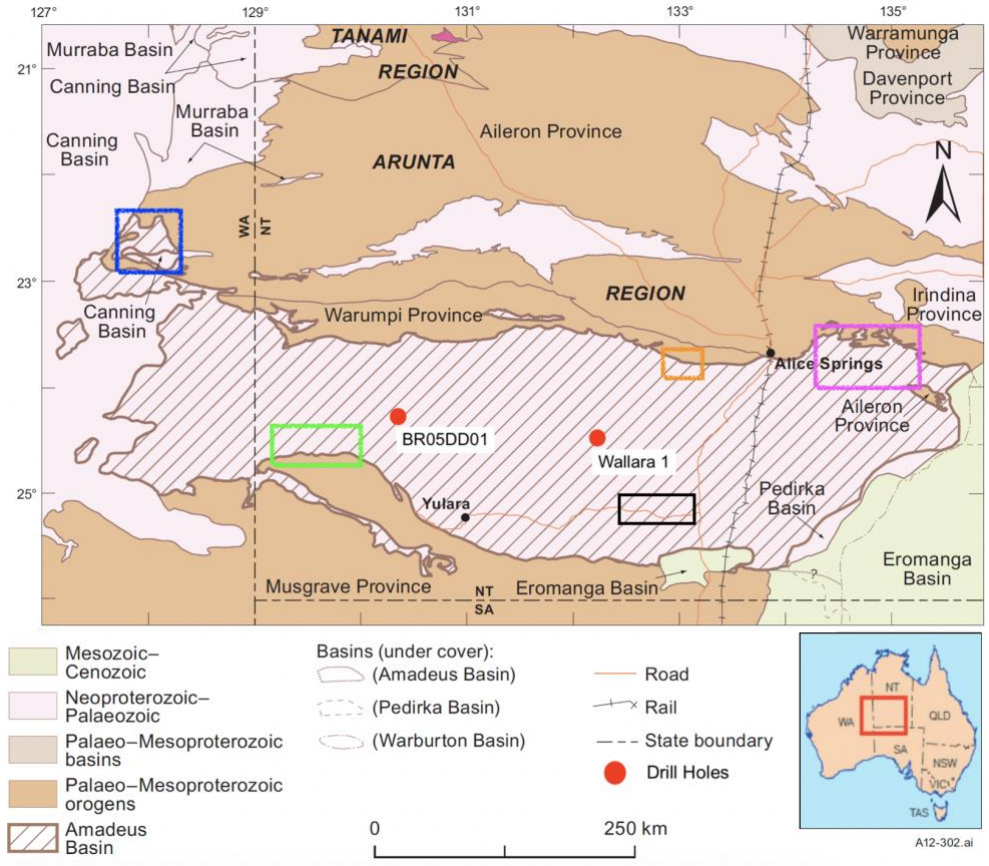

Figure 1: Regional geological setting of Amadeus Basin and surrounding regions. Location of study area shown by black rectangle. Previous study locations shown in blue (Haines & Wingate, 2007), green (Camacho, 2002), orange (Buick, 2005) and purple (Zhao, 1992). The Tanami and Arunta regions are situated in the northern part, Musgrave Province in the southern part of Amadeus Basin. Western Australia Geological regions simplified and slightly modified from Tyler and Hocking (2001).

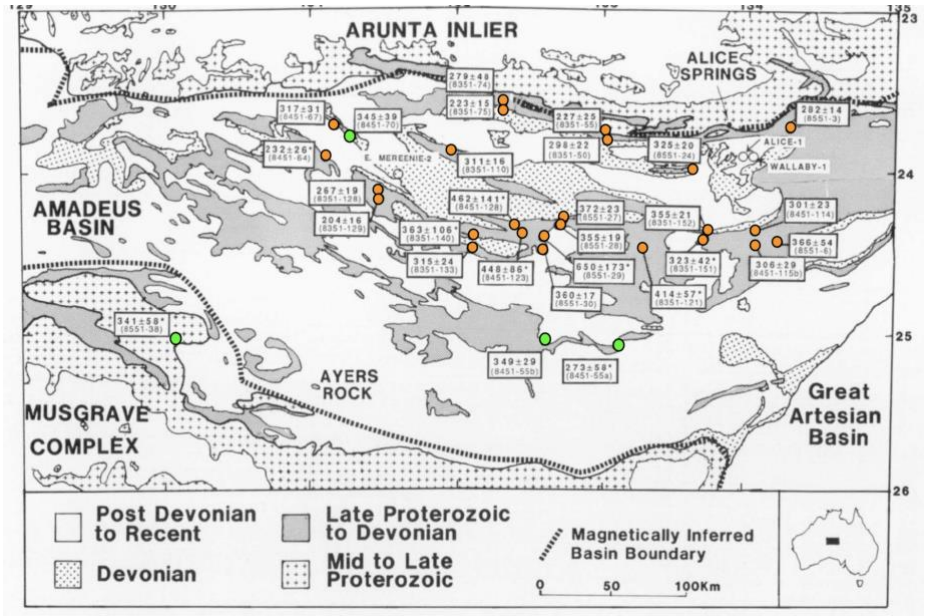

Figure 2: Apatite Fission track ages of outcrop and drill-core samples of Pacoota Sandstone (orange) and Stairway Sandstone (green) (modified from Tingate, 1991).

[2] GEOLOGICAL BACKGROUND

[2.1] Centralian Superbasin

The Centralian Superbasin consisted of several sedimentary basins that covered extensive areas of northern, central and southern Australia during the Neoproterozoic and early Palaeozoic (Munson et al., 2013). Neoproterozoic successions in the Amadeus, Georgina, Ngalia, Officer and former Savory basins share a common, extensive intracratonic depositional system, which forms the Centralian Superbasin (Waleter et al., 1995). The Neoproterozoic Centralian Superbasin, prior to the disruption of the 580 – 530 Ma Petermann Orogeny, is referred as the Centralian A Superbasin. The subsequent, early Palaeozoic depositional system in both central and northern Australia, is referred to as the Centralian B Superbasin.

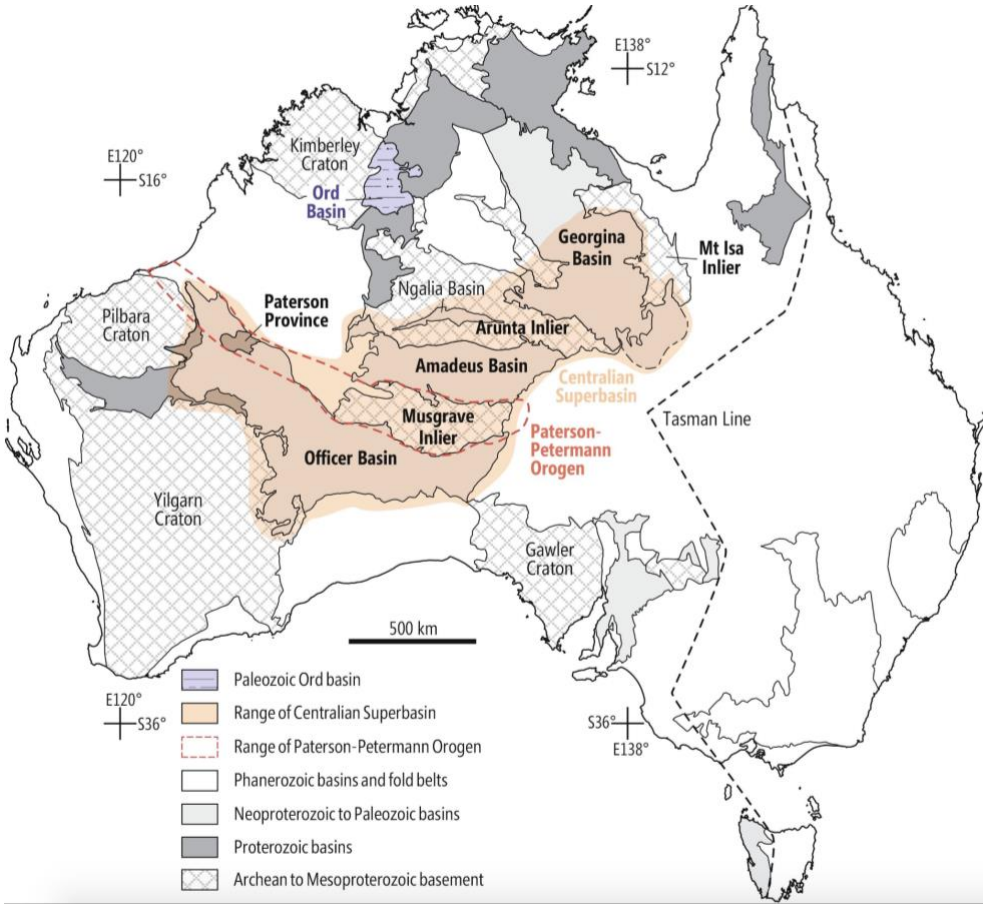

Figure 3: Map location of Centralian Superbasin, sedimentary basins in mainland Australia and basement elements. Modified from Walter *et al.* (1995)

[2.2] Amadeus basin

The large intracratonic Amadeus Basin covers the basement of the Warumpi and Aileron Provinces (Arunta Region) to the north and Musgrave Province to the south (Figure 1). Sedimentation in the basin began in the Neoproterozoic and lasted until the Late Devonian and Early Carboniferous (Edgoose, 2013). Up to 14 km of sediments are preserved in the basin's northern margin and sedimentary thickness is on average ~6 – 12 km in the northern troughs and sub-basins. The southern part of the Amadeus Basin forms a broad and relatively shallow basin and has a maximum total thickness of 3 – 4 km within the central ridge (Wellman, 1991) (Figure 4). Several studies of U-Pb dating of detrital zircons and Sm-Nd isotopes have identified two dominant sources for sediments in the Amadeus Basin; the Arunta region to the north and the Musgrave Province to the south (Figure 4) (Zhao et al., 1992; Camacho et al., 2002; Maidment, 2005; Maidment et al., 2007; Haines et al., 2012b).

The tectonic evolution of the Amadeus basin is complex and was influenced by large-scale intracratonic tectonics and by halo-tectonics (Edgoose, 2013). The northern margin of the Amadeus Basin was tectonically modified during the ~450 – 300 Ma Alice Springs Orogeny. The southwestern basin margin was strongly deformed during the Petermann Orogeny whereas no Alice Springs Orogeny structures have been identified. However, the southeastern basin margin is tectonically unmodified in the present-day surface geology. In contrast, Petermann Orogeny structures are lacking in the northern region and only a few areas in the northwestern region have seen the combined reworking of the Petermann and Alice Springs orogenies expressed by dome-

and-basin fold patterns, formed during the interaction of the two orogenies (Flöttmann et al., 2004).

The Neoproterozoic and Early Palaeozoic successions have been influenced by halo-tectonics, mainly in the northeastern of Amadeus Basin. In more detail, the Neoproterozoic Bitter Springs Formation and Cambrian Chandler Formation are generally associated with evaporites. Due to the salt withdrawal, the effects of diapiric growth and local facies and structures in the Late Neoproterozoic successions led to normal faulting and syn-sedimentary thickening of adjacent units (Kennedy, 1993). The influence of gravity gliding, gravity spreading and salt withdrawal resulted in the series of salt nappe complexes and mini-basins during the Neoproterozoic and early Palaeozoic sedimentation in the Amadeus Basin (Dyson and Marshall, 2007).

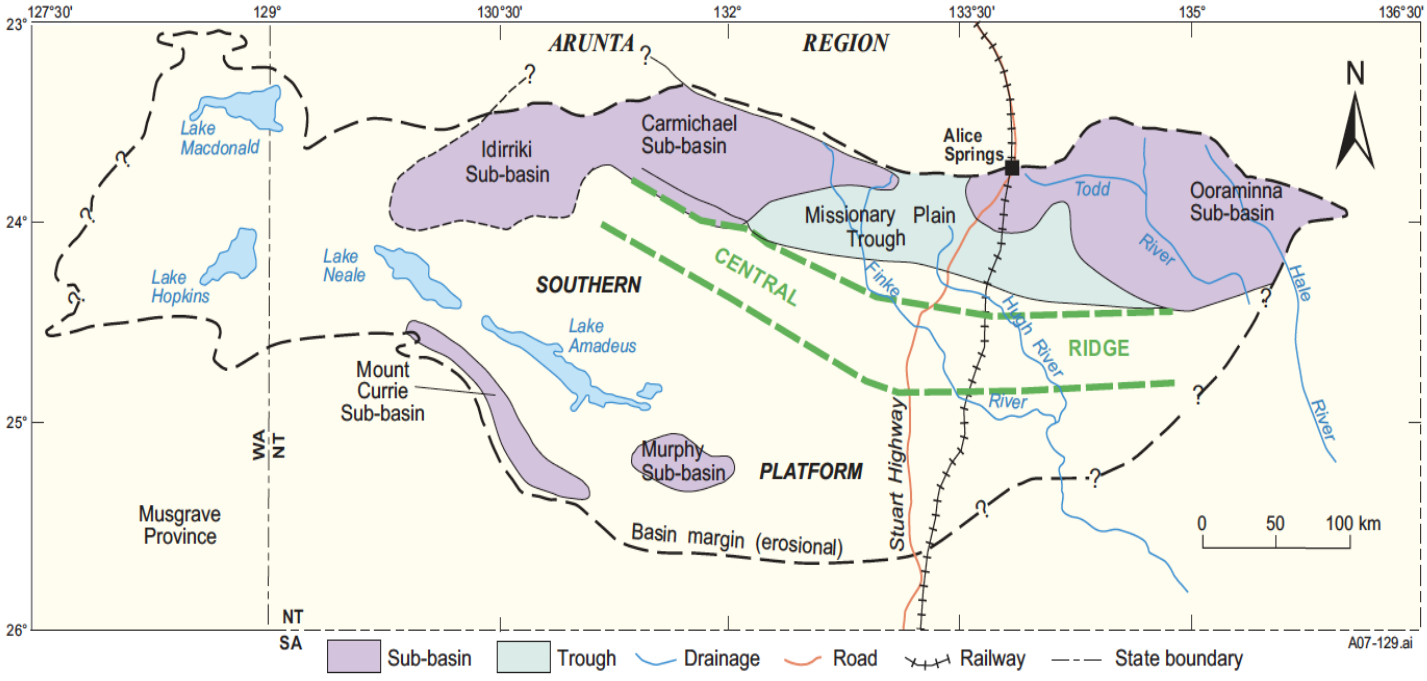

Figure 4: Architecture of Amadeus Basin, showing the northern and southern platform, Central Ridge, sub-basins and Southern Platform elements. (modified from Marshall et al., 2007)

[2.3] Neoproterozoic to early Cambrian sedimentary history

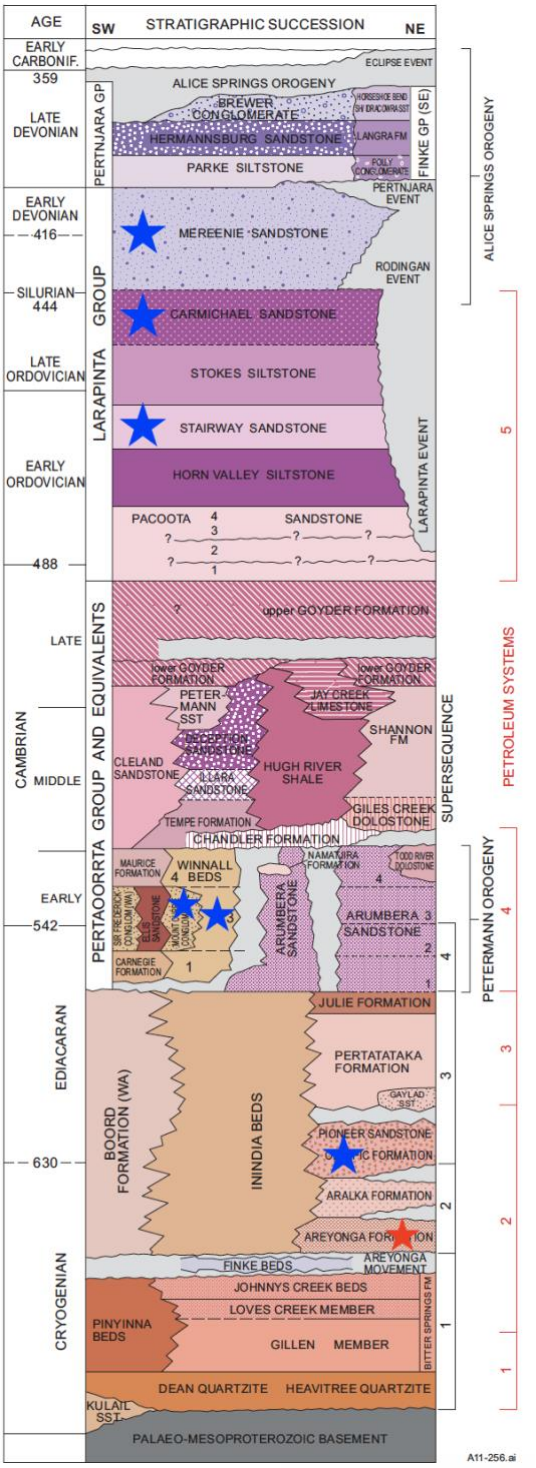

Figure 5: Stratigraphic succession of the Amadeus Basin (Edgoose C.J., 2013) Superseuqences and known petroleum systems shown on the right (Walter et al., 1995; Marshall, 2003; Marshall et al., 2007). Sampled formations for zircon U-Pb are shown by blue stars. Sampled formations for apatite FT and U-Pb are shown by red stars.

Walter *et al.* (1995) subdivided the Neoproterozoic stratigraphic succession of the Amadeus Basin into four supersequences. Supersequence 1 consists of a kilometer of marine and lacustrine carbonates, fine siliciclastics and evaporites. The base of Supersequence 1 is marked by a regional inconformity above a basal quartz arenite succession (Dean Quartzite and Kulail Sandstone in the south, Heavitree Quartzite in the north). Supersequence 2 is marked by the Sturtian glacial sediments, overlying marine shales and carbonates. Supersequences 3 is composed of Marinoan glacial deposits with turbiditic sands and pelagic shales over most of the Superbasin. This supersequence has the presence of very large sphaeromorph and acanthomorph acritarchs which is characterized as the 'Pertatataka microbiota' from the *Pertatataka Formation.* Both Supersequence 2 and 3 are overlain by shallow marine siliciclastic and carbonate successions. Supersequence 4 comprises of widespread marine sands and silts and immature deltaic to non-marine siliciclastic rocks spanning across the Neoproterozoic – Cambrian boundary. The Petermann Orogeny resulted in the termination of sedimentation at ~540 Ma (Maboko et al., 1992).

[2.4] Petermann Orogeny

The Petermann Orogeny (580 – 530 Ma) was a major intraplate tectonic event that introduced high pressure and temperature (granulite and sub-eclogite facies) metamorphism, ductile flow and extreme basin inversion as well as the uplift and the exhumation of the Mesoproterozoic Musgrave Province (Scrimgeour and Close, 1999; Camacho and McDougall, 2000; Raimondo et al., 2010; Aitken et al., 2009; Gregory et al., 2009; Walsh et al., 2012). This tectonic event separated the Neoproterozoic Centralian A Superbasin into the Officer and Amadeus basins to the south and north of the Musgrave Province. The main tectonic model for the Petermann Orogeny is the rapid burial and exhumation in a transpressional, crustal-scale flower structure (Camacho and McDougall, 2000).

At least three phases of folding are recorded in this orogenic event, involving both basement and sedimentary rocks along the southwestern margin of the Amadeus Basin during the early phase (Scrimgeour et al., 1999; Edgoose et al., 2004). Exhumation of basement and sedimentary rocks of Supersequence 1 from mid crustal levels were initiated by large detachment zones which transported a large-scale basement wedge to the north and significant back thrusting of Supersequence 2 and 3 sedimentary rocks to the south to accommodate the shortening (Edgoose, 2013). Furthermore, the Amadeus Basin architecture is majorly disrupted by the Petermann Orogeny, developing large sub-basins and troughs north of the central ridge and a southern platform (Figure 4).

The Petermann Nappe Complex, situated along the northern margin of the Musgrave region, interacts between the Amadeus Basin and Musgrave basement. The formation of the Petermann Nappe Complex resulted from the progressive north-vergent crustal shortening that inserted an internally duplex basement wedge into the

lower Amadeus Basin succession along a basal decollement horizon (Edgoose et al., 2004). The nappe complex is locally unconformably overlain by flat-lying to gently dipping Ordovician shallow-marine sediments (Flöttmann et al., 2004). Amadeus Basin rocks shifted southwards over the inserted basement wedge due to an upper detachment zone (Bloods Backthrust Zone). At the same time, Amadeus Supersequence 1 rocks were buried to more than 20 km and metamorphosed, along with the basement, up to lower to middle amphibolite facies (Edgoose et al., 2004; Flöttmann et al., 2004). The Neoproterozoic Amadeus Basin sediments are mostly unmetamorphosed and gently deformed in the northern part of Bloods Backthrust Zone. This deformation affects the Supersequence 4 formations and older Amadeus Basin units. Depositional loci in the basin progressively moved northwards and sedimentation was focused in these major depocenters. A total of 1500 m clastic sediments were deposited into the Missionary Plains Trough and 2800 m into the Carmichael Sub-basin (Lindsay, 1993; Ambrose, 2006).

Radiometric dating (U-Pb, Rb-Sr, K-Ar) dated the age of Petermann Orogeny ranging between 570 – 530 Ma in Western Australia (Howard et al., 2015) and 580 – 530 Ma in the Northern Territory (Close, 2013). The Petermann Orogeny has been dated to be contemporaneous with the ca. 560 Ma King Leopold Orogeny (southwest Kimberley region) and the ca. 550 Ma Paterson Orogeny (Paterson Region) (Bagas, 2004; Czarnota et al., 2009; Tyler et al., 2012). Therefore, these orogenic domains may be linked beneath the cover of younger sedimentary basins.

[2.5] Alice Springs Orogeny

The Alice Springs Orogeny (450 – 300 Ma) was a major intracontinental event that affected the Central Australian region by uplifting and exhuming the Arunta Region and inducing substantial deformation in the northern Amadeus Basin (Edgoose et al., 2013a). Deep crustal rocks were exhumed ~40 km to be juxtaposed against upper crustal Proterozoic basement and sediments of the Amadeus Basin, exposing the Arunta Province. Earlier phases of this orogeny are mainly discrete events and related to unconformities within basin successions. In addition, a Late Devonian phase in the Amadeus Basin resulted in basin inversion and termination of Palaeozoic deposition. The Alice Springs Orogeny caused crustal shortening with estimates ranging from 50 km (Flöttmann et al., 2004) to 60 – 125 km (Haines et al., 2001) and the orogeny also accounts for most geological structures (domes, folds and thrusts) in the present-day surface geology of the Amadeus Basin.

This long-lived orogeny of 150 million years can be subdivided in three times of peak tectonic activity: the Rodingan Event (450 – 440 Ma), the Pertnjara – Brewer Event (390 – 375 Ma) and the Eclipse Event (340 – 320 Ma). The Rodingan Event is expressed as an unconformity between the Mereenie and Carmichael Sandstones in the north and northeast of the basin (Shaw, 1991; Bradshaw and Evans, 1988) (Figure 5). This unconformity cuts down at a low-angle through the succession to the northeast and coincides with the end of marine sedimentation in the basin (Edgoose et al., 2013a). The Rodingan Event is identified as the first Palaeozoic compressional event in the Amadeus Basin (Shaw et al., 1991). This event triggered the localized basin inversion towards the northeast and was succeeded by deposition of immature sediments of the deltaic Carmichael Sandstone (Haines et al., 2001). The Pertnjara Event induced an

unconformity between the Mereenie Sandstone and Pertnjara Group in the northeast and central-north of the basin. The Brewer Event in the northeast of the basin induced substantially uplift and erosion, resulting in the removal of ~ 1200 m of Hermannsburg Sandstone followed by deposition of the Brewer Conglomerate (Jones, 1972; Bradshaw and Evans, 1988). These Pertnjara and Brewer events correspond to the Devonian period of major thick-skinned structures in the Arunta Region.

[2.6] Sample Locations

[2.6.1] Outcrop Samples

Nineteen outcrop samples from the Neoproterozoic, Cambrian, Ordovician and Silurian-Devonian were collected from the KULGERA region in the Southern Amadeus Basin, in order to determine their provenance and thermal history (Figure 6). The Line 9 (with L9 prefix) and Basedow Range (with BD prefix) outcrop samples are located in the northwestern part of the KULGERA region, and the Costellos Bore (CB prefix) and Erldunda Range (E prefix) samples are situated in the northeastern part. A total of eight BD, seven R, two L9, and two CB outcrop samples were analysed for zircon U-Pb geochronology. Their depositional ages are mainly Ordovician and Cambrian, with some samples sourced from Silurian-Devonian and Neoproterozoic successions. The Ordovician samples were taken from the Larapinta Group, being either Carmichael or Stairway Sandstone. The Neoproterozoic and Cambrian samples are from the Pertaoorrta Group, Winnall Group and Pioneer Sandstone and one sample was sourced from the Mereenie Sandstone with Silurian-Devonian age (Figure 5).

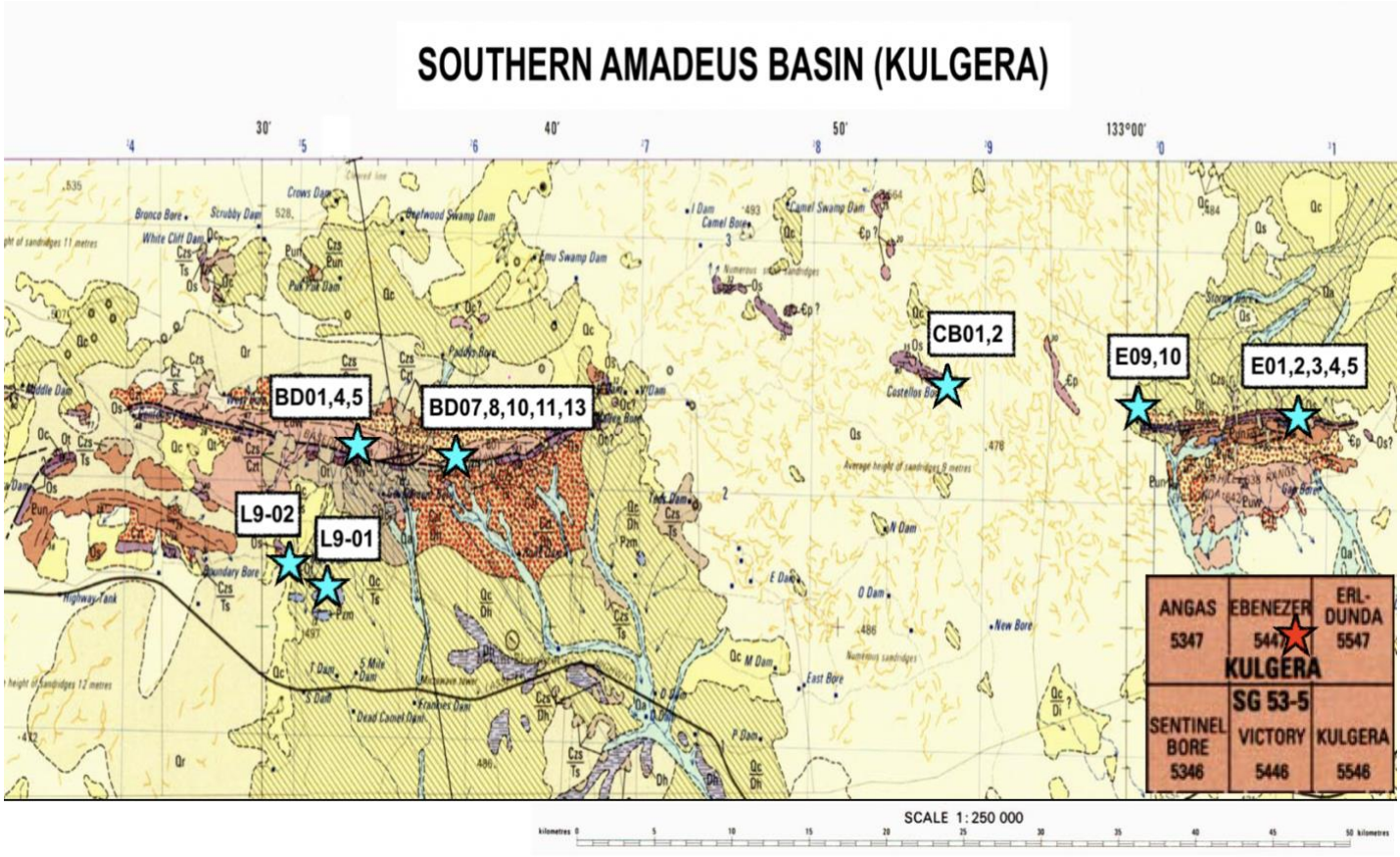

Figure 6: Map of the zircon study area, Southern Amadeus Basin, KULGERA with indication of sample locations. Outcrop sample locations shown in blue stars. Specified location within KULGERA where samples were collected is shown in red star, (Ebenzer, 5447). (NTGS, 1992)

[2.6.2] Drill Core Samples

Eight drill core samples were collected from the BR05DD01 well (S24º27'20.95, E130º22'57.0) located in the southwestern region of the Amadeus Basin (Figure 1) for apatite 'double dating' (fission track + U-Pb). This well has a total depth of 1224.98 meters and cuts through Neoproterozoic sediments (Cryogenian – Ediacaran). The Cryogenian sediments are composed of Johnnys Creek Beds, the Loves Creek Member and the Bitter Springs Formation. The Edicaran sediments are part of the Pertatataka and Areyonga Formations. Unfortunately, only two of the eight drill core samples (B3 and B12) could be analysed due to very poor apatite yields in the remaining six samples. The B3 sample were retrieved at 507.5 – 509.5 m depth and the

B12 sample at 523.8 – 525.8 m depth, both classified as Areyonga Formation. Given that both samples are sourced from the same formation with limited depth difference and rather poor apatite yields, they have been combined to one sample for this thesis.

[2.7] Sedimentary geology of the sampled formations

[2.7.1] Mereenie Sandstone

The fine to medium grained Mereenie Sandstone is thinly to thickly bedded and comprises white to pale brown, very quartz sandstone (Figure 5). Weathered surfaces are often medium brown to orange-red (Appendix A) (Edgoose et al., 2013). It is a very widespread unit in the basin, with a present-day north-south extent of ~200 km and east-west extent of ~800 km. The Mereenie Sandstone has a variable depositional environment with the upper part in an aeolian-fluvial settings and the lower part deposited under shallow marine conditions (Kennard and Nicoll, 1986). Ripple marks are common, mostly symmetrical ripples, in the lower part of this succession. The Mereenie Sandstone lays conformably above the Carmichael Sandstone.

[2.7.2] Carmichael Sandstone

The very fine to medium grained Carmichael Sandstone, underlying the Mereenie Sandstone, comprises interbedded pale brown to red-brown sandstone, siltstone and mudstone (Figure 3 and Appendix A). It is poorly exposed in the central and western region and absent in the eastern region where it is either eroded prior to deposition of overlying Mereenie Sandstone or was never deposited. The Carmichael Sandstone has about 150 m thickness in the southern part and 100 m thickness in the northern part (Kennard and Nicoll, 1986). Trough and tabular cross-beds are common

and different characteristics of sandstones illustrates a mixed depositional environment including shallow marine to possible hypersaline and fluvial conditions (Edgoose et al., 2013).

[2.7.3] Stairway Sandstone

The widespread Stairway Sandstone lies disconformable above the Horn Valley Siltstone in the northern part of the basin and unconformable on the Cambrian Pertaoorrta Group in the southern part. The Stairway Sandstone is subdivided into three units (Figure 5) (Cook, 1972); the upper unit is characterized by thinly bedded quartzic sandstone with interbeds of siltstone and mudstone, and rare phosphorites. The middle unit consists mostly of thinly bedded sandstone with residual phosphatic gravels and some fossils. The lower unit is massively bedded quartzic sandstone with abundant sedimentary structures and ichnofossils (Edgoose et al., 2013). The Stairway Sandstone is thought to be deposited in a broad epicontinental seaway. Attributable to the abundance of fossils, the upper unit indicates deeper water conditions, whereas both middle and lower units likely deposited in shallow subtidal and partly intertidal conditions (Appendix A) (Kennard and Nicoll, 1986).

[2.7.4] Winnall Group, Froud and Liddle Formations

The Winnall Group was previously defined as Winnall beds by Ranford *et al* (1965) and this group comprises of newly defined Breaden, Gloaming, Froud, Liddle and Puna Kura Kura Formations (Donnellan and Normington, 2017). The Winnall Group is informally divided into lower (Breaden, Gloaming and Froud formations) and upper (Liddle and Puna Kura Kura formations) successions. The lower Winnall Group

is likely to correlate with the Petertatataka Formation and the upper group has a correlation with the Arumbera Sandstone (Haines et al., 2010, 2012).

The Liddle Formation is a fine-grained, thinly planar-parallel bedded and laminated, reddish-brown and grey-green sandstone. The depositional environment for the Liddle Formation is shallow marine or intertidal. The underlying Froud Formation comprises thinly bedded, laminated sandstone. The depositional environment is inferred to be off-shore on the basis of the paucity of shallow marine to intertidal sedimentary structures that characterize the underlying and partially laterally equivalent Breaden Formation (Figure 5 and Appendix A).

[2.7.5] Mount Currie Conglomerate (Pertaoorta Group)

The large conglomeratic unit (~1.5 m) of Mount Currie Conglomerate comprises a thick succession of coarse pebble, cobble and boulder conglomerate (Figure 5). The clasts are predominantly of felsic volcanic rocks, which are un-deformed and locally strongly epidotised. The clasts are furthermore subrounded to rounded and locally up to 70 cm in diameter with median size of 15 – 20 cm (Appendix A) (Sweet *et al*., 2012). Many studies have proposed that the Mount Currie Conglomerate is a proximal foreland succession deposited in a piedmont setting, resulting from the uplift of Musgrave Province and overlying Neoproterozoic units during the Petermann Orogeny (Forman 1965, Wells et al 1970, Sweet and Crick 1992).

[2.7.6] Pioneer Sandstone

The fine to medium grained feldspathic and arkosic Pioneer Sandstone is restricted to the central-northern part of Amadeus Basin (Figure 5 and Appendix A). This sandstone was deposited in a shallow marine and tidal environment. The upper part

of the sandstone is dolomitic and has abundant tabular cross-beds, whereas the lower part is white, feldspathic and dominantly planar laminated, some with cross-laminations in 10 cm deep channels (Walter and Bauld, 1983). This sandstone is interpreted to be an intertidal, periglacial or glacial outwash facies that correlates with Olympic Formation diamictite in the eastern Amadeus Basin (Preiss et al 1978, Walter et al 1995).

[2.7.7] Areyonga Formation

The thinly interbedded sandstone, conglomerate, shale, siltstone and dolostone Areyonga Formation is mostly exposed in the central, north and northeastern region of the Amadeus Basin (Figure 5). The sandstone unit in this formation is coarse to very coarse-grained with rounded to angular grains. The sandstone beds are likely representative of a fluvioglacial depositional setting or a relatively small ice cap, concentrated from two parts of ice in the northeast of the basin. The deposition was controlled by basin dynamics and eustatic sea level changes resulting from the global ice age (Lindsay, 1989). The Areyonga Formation correlates with other Neoproterozoic glacial successions in the Adelaide Fold Belt, Georgina and Ngalia basins, and also in Kimberley region of Western Australia (Priess et al., 1978).

[3] METHODS

[3.1] Laboratory Processing

Apatite and zircon samples were prepared using conventional crushing and separation techniques. The heavy fraction was separated from the light mineral fraction through panning process and passing the heavy fraction through the Frantz magnetic separator at 1.6 amp. The remaining non-magnetic heavy minerals were separated through LST Heavy Liquid (*2.85 ± 0.02 g/ml*). Subsequently, apatite and zircon samples were mounted in EpoxyCure resin, grounded with #2000 carbide paper and polished with 1 μm and 3 μm diamond paste. Polished apatite samples were etched in 5 M HNO_3 nitric acid for 20.0 ± 0.5s at 20.0° ± 0.5°C to expose the spontaneous fission tracks. The samples were gold coated for apatite and carbon coated for zircon samples.

[3.2] Zircon U-Pb geochronology

The zircon grains were imaged with a Cathodoluminescence (CL) detector on a FEI Quanta600 Scanning Electron Microscope operating at 15 kV and 6.5 mA to examine the internal zircon structures and to be used as a guide for analytical laser spot locations. Subsequently, the zircons were analysed for their U and Pb isotopic compositions using Laser Ablation Inductively Coupled Plasma Mass Spectrometry (LA-ICP-MS) with a New Wave 213 laser coupled to an ICP-MS Agilent 7900x mass spectrometer. Ablation spot diameters of 30 μm, energy pulses of 4 $J.cm^{-2}$ and repetition rates of 5 Hz were used. Every 15 zircon spots were interspaced between two GJ-1, two Plešovice and a 91500 zircon standard analyses. GEMOC GJ-1 zircon, with TIMS ages of $^{207}Pb/^{206}Pb$ = 607.7 ± 4.3 Ma, $^{206}Pb/^{238}U$ = 600.7 ± 1.1 Ma and $^{207}Pb/^{235}U$ = 602.0 ± 1.0 Ma, was used as the primary zircon standard to correct for U-Pb and laser-induced

fractionation and for instrumental mass discrimination (Jackson et al, 1994). The Plešovice zircon (ID TIMS $^{206}Pb/^{238}U$ age = 337.13 ± 0.37 Ma) and 91500 zircon ($^{206}Pb/^{238}U$ age = 1062.4 ± 0.4 Ma) internal standards were used to examine the accuracy and precision of the measurements (Sláma et al, 2008).

Data reduction was carried out using Iolite software and isotopic ratios were plotted on concordia graphs using the Microsoft Excel add-in Isoplot (Ludwig, 1999). $^{206}Pb/^{238}U$ ages were chosen as the best estimate of the age of the detrital zircons that are younger than 1.3Ga. The $^{207}Pb/^{206}Pb$ age was used for older zircons (Spencer et al., 2016). The threshold that separates concordant from discordant zircons was set at 10% discordance. Kernel density estimates (KDE) and probability density plots (PDP) were plotted through the program Density Plotter (Vermeesch, 2012). These plots enable to visualize detrital age distributions. The KDE function stacks a Gaussian 'bell curve' on top of each measurement and the standard deviation is determined by the local probability density. The PDP also stacks Gaussian 'bell curves' on top of each measurement but standard deviation is determined by the analytical precision (Vermeesch, 2012).

[3.3] Apatite Fission Track and U-Pb thermochronology

Each mounted apatite grain was imaged on a Zeiss AXIO Imager M2m Autoscan System using TrackWorks software. Both confined track lengths and surface track densities were calculated using FastTracks software. Subsequently, U and Pb isotopes were measured using the same analytical procedure as explained above for the zircon analyses. The Madagascar apatite was used as the primary standard (ID-TIMS U-Pb age of 473.5 ± 0.7 Ma; Chew et al., 2014) for U-Pb analysis and NIST 610 as the primary standard for the U concentration measurements required for the AFT age

calculations. In order to test the accuracy of results, Durango apatite ($^{40}Ar/^{39}Ar$ age of 31.44 ± 0.18 Ma; McDowell et al., 2005) and McClure apatite (TIMS U-Pb age of 523.51 ± 1.47 Ma; Schoene and Bowring, 2006) were used as secondary standards. Apatite U-Pb isotopic ratios were plotted on a Terra-Wasserburg Concordia plot (Vermeesch, 2012). After linear regression, the lower intercept was used to determine the apatite U-Pb age. Fission track ages were plotted on a radial plot, Java plugin RadialPlotter to determine the AFT central age and to identify (potentially) multiple age populations (Vermeesch 2009, 2017).

LASER	
Type	Nd:YAG
Brand and Model	ESI NWR213
Wavelength	213 nm
Pulse Duration	~ 4 ns
Repetition Rate	5 Hz
Spot Size	30 μm
Laser Fluence	~ 4 $J.cm^{-2}$
ICP-MS	
Brand and Model	Agilent 7900x
Forward Power	1350 W
Torch Depth	4.5 mm
GAS FLOWS (L/min)	
Carrier (He)	0.7
Sample (Ar)	0.88
DATA ACQUISITION PARAMETERS	
Data Acquisition Protocol	Time - resolved analysis
Scanned Masses	U^{238}, Pb^{204}, Pb^{206}, Pb^{207}, Pb^{208}, Th^{232}, Si^{29}, Cl^{35}, Ca^{43}, Mn^{55}, Sr^{88}, Y^{89}, Hg^{202}
Detector Mode	Peak hopping, pulse and analogue counting
Background Collection	30 seconds
Ablation for Age Calculation	30 seconds
Washout	20 seconds
STANDARDS	
Primary Standards	GJ1, Madagascar Apatite, NIST 610
Secondary Standards	Plešovice, 91500, Durango Apatite, McClure Apatite

Table 1: Analytical details for LA-ICP-MS analysis used

[4] RESULTS

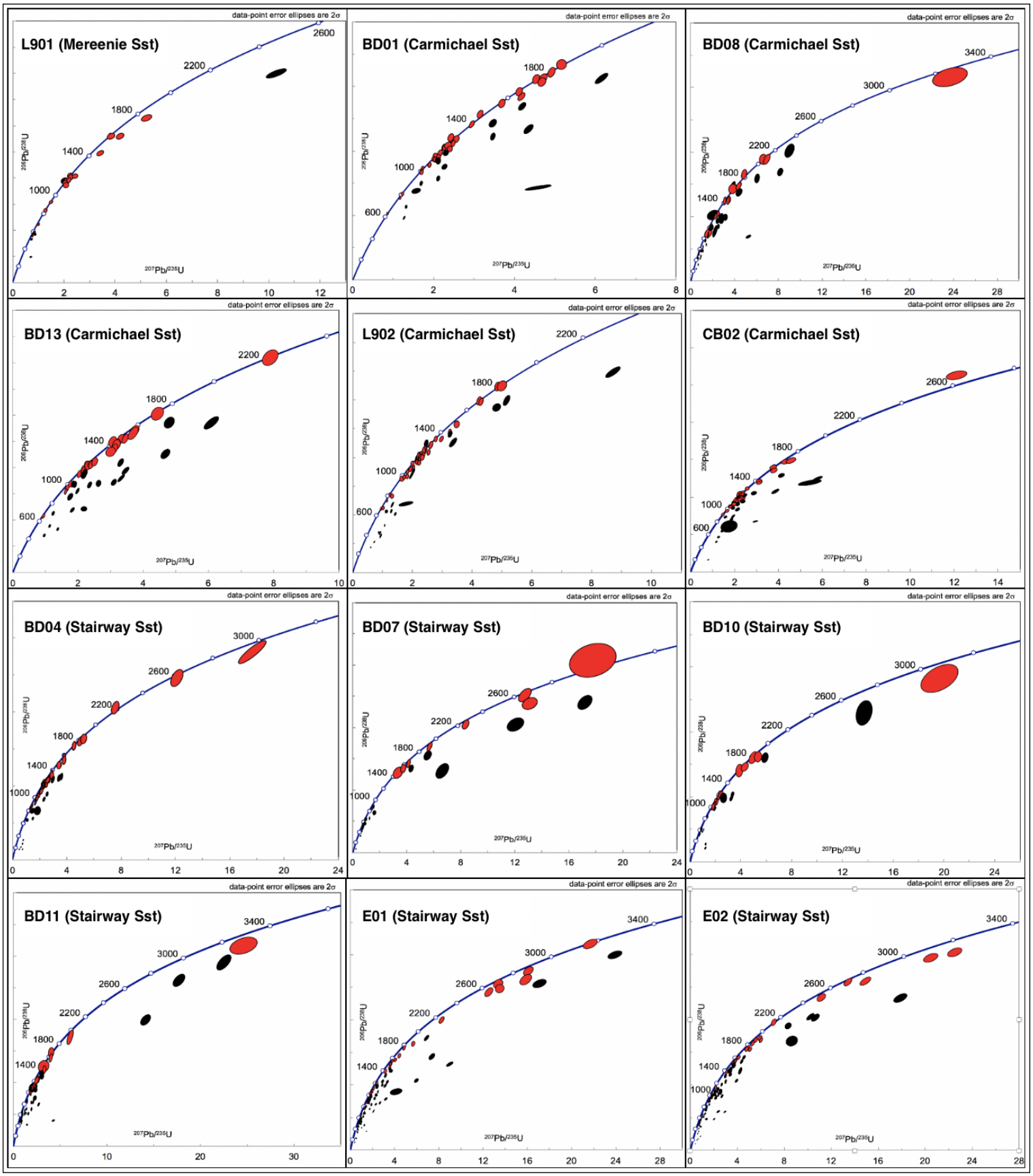
data-point error ellipses are 2σ
L901 (Mereenie Sst)
BD01 (Carmichael Sst)
BD08 (Carmichael Sst)
BD13 (Carmichael Sst)
L902 (Carmichael Sst)
CB02 (Carmichael Sst)
BD04 (Stairway Sst)
BD07 (Stairway Sst)
BD10 (Stairway Sst)
BD11 (Stairway Sst)
E01 (Stairway Sst)
E02 (Stairway Sst)
207Pb/235U
206Pb/238U

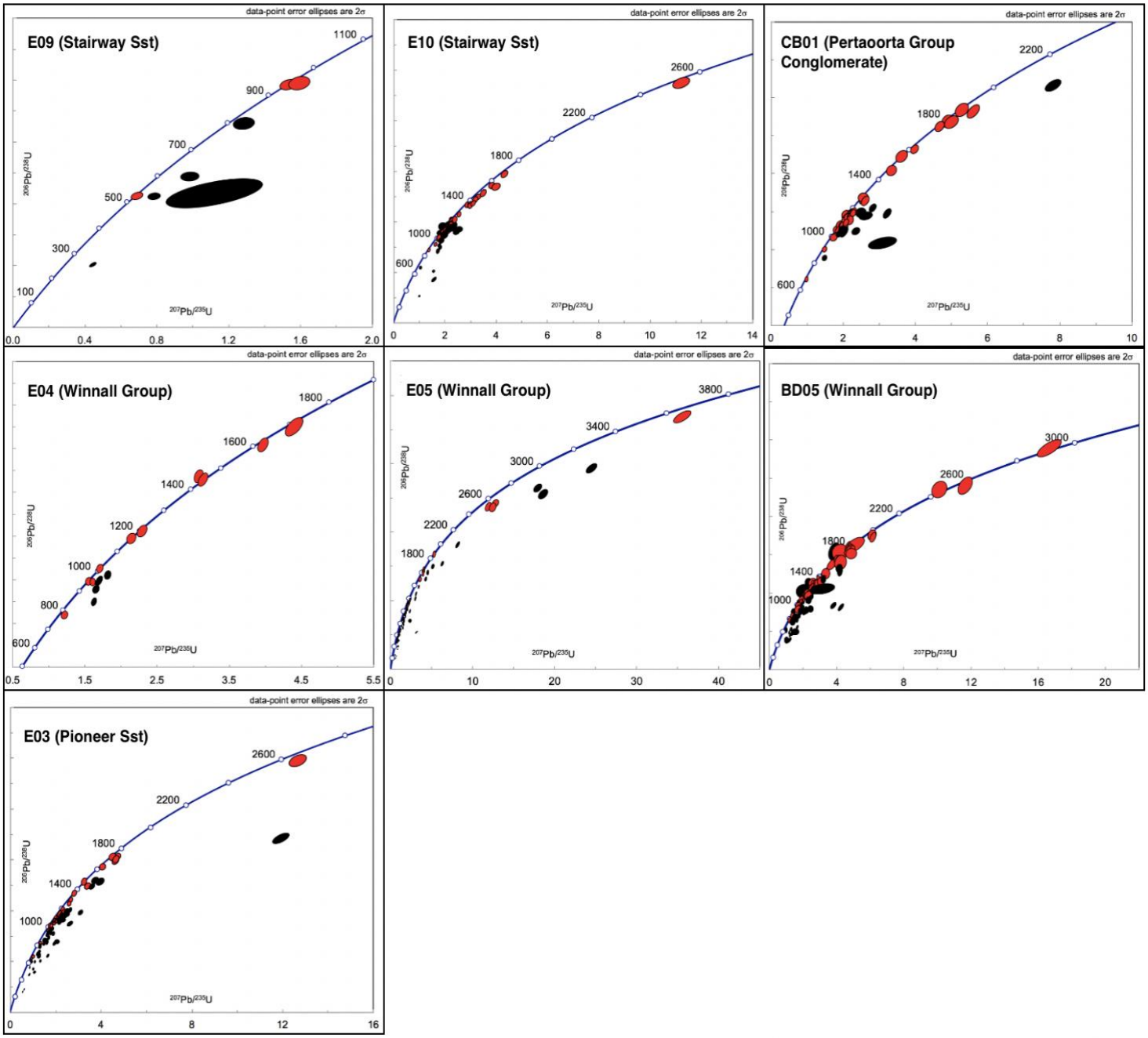

Figure 7: Wetherill U-Pb Concordia plots of 19 samples taken from the Southern Amadeus Basin. Error ellipses are the 2 standard deviation level. Sample locations are given in Figure 6 and Table 1. Red ellipse = within 10% concordance threshold, black ellipse = discordant. Concordia plots using the Microsoft Excel add-in Isoplot (Ludwig, 1999)

Stratigraphic Unit	Sample	Lithology	Location	Major U-Pb detrital age peaks (Ma)	No. of U-Pb analyses	No. of 10% concordant U-Pb analyses	Youngest 10% concordant U-Pb analysis (Ma)
Mereenie Sst	L901	Red brown, fine- to medium-grained sandstone	S25º09'14.8" E132º31'59.6"	582, 1156, 1595	25	19	554 ± 10
Carmichael Sst	BD01	Pale grey, very fine-grained sandstone	S25º06'14.4" E132º32'51.2"	1166, 1778	44	29	635 ± 12
Carmichael Sst	BD08	Pale grey, fine-grained sandstone	S25º06'32.7" E132º36'12.9"	476, 957, 1581	50	19	455 ± 13
Carmichael Sst	BD13	White – pale grey, banded medium-grained sandstone	S25º06'19.7" E132º37'05.4"	1197, 1482	45	24	662 ± 21
Carmichael Sst	L902	Pale grey, fine- to medeium-grained sandstone	S25º08'29.4" E132º30'56.7"	1179	59	40	680 ± 12
Carmichael Sst	CB02	Clear - pale grey, medium-grained sandstone	S25º04'47.1" E132º53'41.8"	1556	72	52	925 ± 15
Stairway Sst	BD04	Clear – light grey, thinly bedded, fine-grained sandstone	S25º05'54.4" E132º32'53.4"	1186	49	33	817 ± 24
Stairway Sst	BD07	Clear – yellow – transparent brown, fine-grained sandstone	S25º06'37.2" E132º36'15.6"	570	35	16	507 ± 16
Stairway Sst	BD10	Pale grey – white, fine-grained sandstone	S25º06'38.2" E132º35'31.6"	1095, 1788	29	16	514 ± 15
Stairway Sst	BD11	Pale grey, very fine-grained siliceous quartzite sandstone	S25º06'35.6" E132º36'14.5"	574, 1103	57	30	501 ± 14
Stairway Sst	E01	White – pale grey, very fine-grained sandstone	S25º05'20.9" E133º05'45.2"	566, 1037, 1597, 2780	110	43	496 ± 9
Stairway Sst	E02	Pale grey, very fine-grained sandstone	S25º05'22.1" E133º05'45.9"	549, 1029, 1646	118	46	480 ± 9
Stairway Sst	E09	Pale grey, very fine-grained sandstone	S25º05'40.3" E133º00'32.0"	526, 940	10	3	529 ± 12
Stairway Sst	E10	Red brown, fine-grained sandstone	S25º05'42.0" E133º00'34.3"	1143	87	68	874 ± 17
Winnall Group – Liddle Beds	BD05	Medium purple – purple red, very fine grading to arenaceous siltstone	S25º05'51.0" E132º32'54.0"	1109, 1671	111	60	793 ± 36
Winnall Group – Liddle Beds	E04	White – pale grey – pale red, very fine- to fine-grained sandstone	S25º06'15.9" E133º06'44.3"	963, 1417	14	10	779 ± 16
Winnall Group – Froud Fm	E05	Red – brown, medium grained sandstone.	S25º06'31.6" E133º06'11.1"	617, 1134, 1584	91	42	491 ± 10
Pertaoorrta Group Conglomerate	CB01	Pale grey, fine- to medium-grained siliceous sandstone	S25º04'49.0" E132º53'42.1"	1134, 1791	47	36	685 ± 16
Pioneer Sst	E03	Red brown – purple, fine- to medium-grained sandstone	S25º05'35.7" E133º06'01.0"	646, 1086, 1740	85	37	624 ± 12

Table 2: Summary of sample details with locations, lithologies and youngest concordant detrital zircon ages.

[4.1] Zircon U-Pb

[4.1.1] Mereenie Sandstone (Silurian – Early Devonian)

Twenty-five zircon grains were analysed for U-Pb from sample L901, nineteen from all zircon grains were within 10% of concordance and show a broad distribution of zircon ages ranging between ~554 and ~1961 Ma (Figure 8). The most prominent age peak was identified at ca. 1156 Ma. Two other age peaks are centered at ca. 582 and ca. 1606 Ma in the kernel density estimate (KDE) plot. The youngest concordant analysis has an age of 554 ± 10 Ma (2σ), providing a maximum depositional age for the sample. All zircon grains in the Mereenie Sandstone are Proterozoic in age. Note that 19 concordant grains are not sufficient for robust provenance interpretations as theoretically 117 grains are required (Vermeesch, 2004), so these data need to be treated with caution in the interpretations below.

[4.1.2] Carmichael Sandstone (Late Ordovician)

Two hundred and seventy zircon grains were analysed for U-Pb from five samples (BD01, BD08, BD13, L902, CB02). One hundred and sixty-four analyses yielded results were within 10% concordance and the resulting ages show a broad age range between ~635 and ~3252 Ma. Twenty-nine near-concordant zircons from sample BD01 yielded ages in the range ~635 – 1840 Ma. There is a major age peak cluster at ca. 1166 Ma and a minor peak at ca. 1778 Ma. Most zircons from sample BD08 yield ages in the range ~455 – 3252 Ma, with a major peak at ca. 1581 and two minor peaks at ca. 476 and ca. 957 Ma. Twenty-four concordant analyses from sample BD13 yielded ages in the range ~662 – 2226 Ma, the majority are Mesoproterozoic with two peaks at ca. 1197 and ca. 1482 Ma. Forty near-concordant zircons from sample L902 yielded

ages between ~680 – 1824 Ma with only one peak at ca. 1179 Ma. Lastly, fifty-two zircon grains in sample CB02 are near-concordant, yielding ages between ~925 – 2548 Ma with a prominent peak at ca. 1556 Ma. The most prominent peak shown in the pooled Carmichael Sandstone KDE plot is centred on ca. 1163 Ma and a less prominent peak at around ca. 1554 Ma. The youngest near-concordant analysis of the Carmichael Sandstone yielded an age of 455 ± 13 Ma (2σ) from sample BD01, providing the maximum depositional age for the formation.

[4.1.3] Stairway Sandstone (Early Ordovician)

Four hundred and ninety-five zircon grains were analysed for U-Pb from eight Stairway Sandstone samples (BD04, BD07, BD10, BD11, E01, E02, E09, E10). Two hundred and fifty-five zircon grains from all are within 10% of concordance and show a broad age range between 480 – 3357 Ma. One major peak centered at ca. 1141 Ma and two minor peaks centered at ca. 550 Ma and 1591 Ma in the KDE plot for this formation. Thirty-three concordant analyses from sample BD04 yield ages in the range 817 – 3022 Ma, with the majority being Mesoproterozoic with a peak at ca. 1186 Ma . Six mid-Archaean to late Palaeoproterozoic grains range between 1626 – 3022 Ma. Sample BD07 comprises sixteen concordant zircon grains with ages ranging from 507 – 2950 Ma and a peak at ca. 570 Ma. Sixteen concordant analyses from sample BD10 yield ages between 514 – 3165 Ma with a major peak at ca. 1095 Ma and minor peak at ca. 1788 Ma. Sample BD11 contains thirty concordant zircon grains, mostly of Proterozoic age and one zircon in the mid-Archaen. This sample has a prominent peak at ca. 574 Ma and less prominent peak at ca. 1103 Ma. All other samples (E01, E02, E09 and E10) yielded similar age range between 480 – 3288 Ma with majority in the

Proterozoic. Twelve Mid to Late Archaen zircons have ages between ca. 2520 Ma and 3288 Ma. Zircons in these samples display a notable age peak at ca. 1134 Ma and two minor peaks at ca. 565 and 1599 Ma. One zircon with an age of 480 ± 9 Ma (2σ) from sample E02 shows the youngest near-concordant analysis, giving the maximum depositional age.

[4.1.5] Mount Currie Conglomerate, Pertaoorta Group (late Neoproterozoic – early Cambrian)

A total of forty-seven zircon grains were analysed and only thirty-six grains fall within 10% concordance. Zircons from this sample are all Proterozoic and range in age between 685 – 1867 Ma. These Proterozoic zircons shows a prominent peak at ca. 1134 Ma and a less prominent peak at ca. 1791 Ma. The youngest concordant analysis yields a date of 685 ± 16 Ma (2σ), providing a maximum depositional age of the sample.

[4.1.4] Winnall Group, Liddle & Froud Formations (late Neoproterozoic – early Cambrian)

Detrital zircons were separated from both the Liddle Formation (samples BD05, E04) and Froud Formation (sample E05). A total of two hundred and sixteen zircon grains were analysed, however, only one hundred and twelve were within 10% concordance. A distinct age peak at ca. 1148 Ma was obtained in addition to two minor peaks at ca. 624 and 1584 Ma. The Liddle Formation yielded ages ranging between 779 – 2879 Ma, most of which are Proterozoic. In the Froud Formation, zircon ages range between 491 – 3697 Ma (Early Cambrian – Late Archean). The youngest near-

concordant age from the Liddle Formation was dated at 779 ± 16 Ma (2σ). For the Froud Formation, the youngest grain is 491 ± 10 Ma (2σ).

[4.1.6] Pioneer Sandstone (late Cryogenian – middle Ediacaran)

A total of eighty-five zircon grains were analysed for U-Pb from sample E03, thirty-seven zircon grains were within 10% concordance. The resulting zircon U-Pb ages range between 624 – 2691 Ma, and are thus all Proterozoic, excluding an older Archean grain. A prominent peak displated in the KDE plot at ca. 1096 Ma was obtained in addition to by two less prominent peaks at ca. 646 and 1740 Ma. The youngest concordant age 624 ± 12 Ma (2σ), providing a maximum depositional age for the sample. As discussed above, caution is required during interpretation of the data for this sample as thrity-seven concordant grains are insufficient for robust provenance interpretations (Vermeesch, 2004).

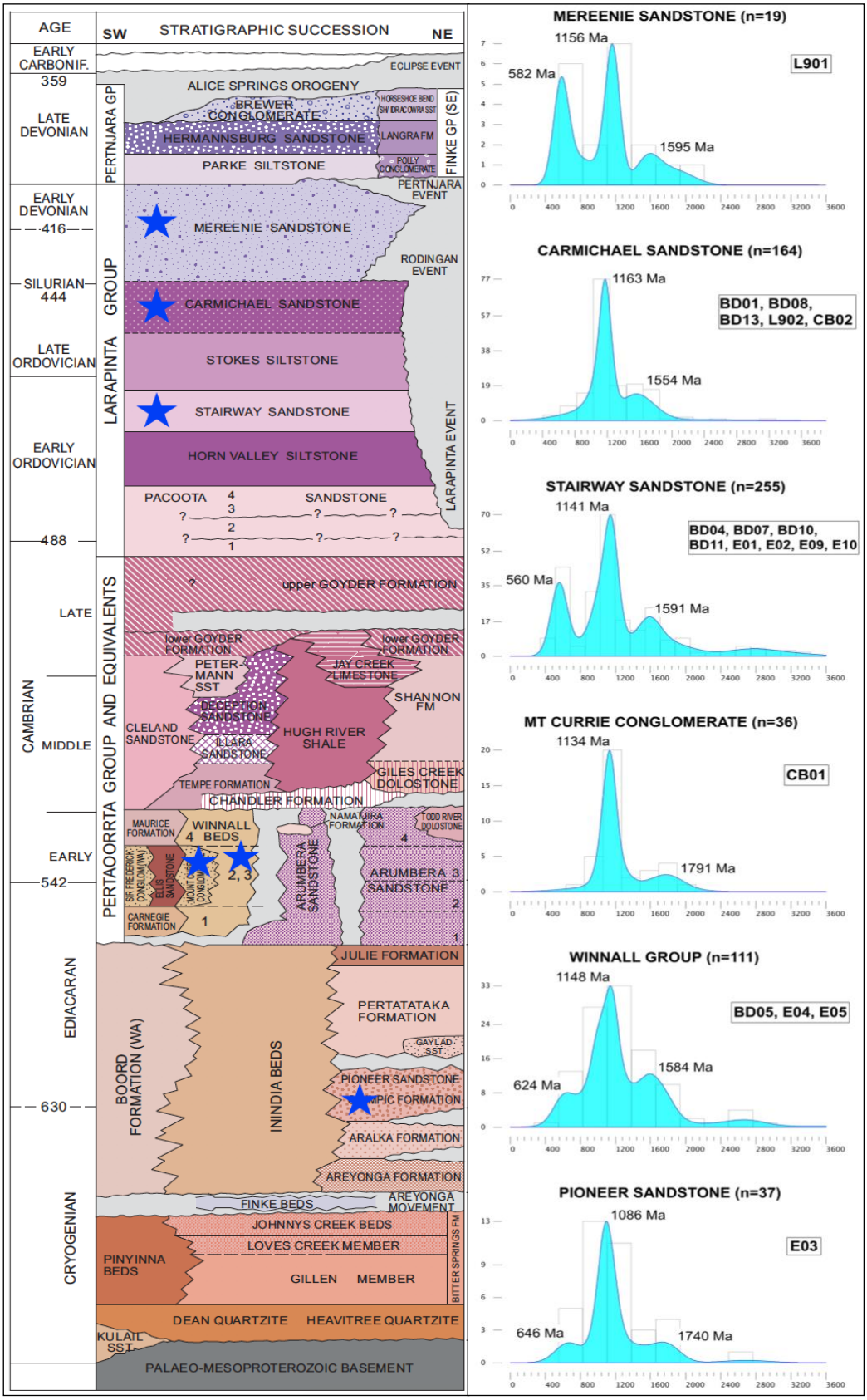

Figure 8: Stratigraphic column of Amadeus Basin and the correlative KDE plots (Density Plotter; Vermeesch, 2012) for all formations analysed in the zircon analysis. Each individual peak and sample ID are labelled in the KDE plots. Blue stars represent the correlative formations.

[4.2] Apatite U-Pb

Figure 9 shows a Terra-Wasserburg Concordia plots for all eight apatite grains analysed from the Areyonga Formation. Four grains plot along a regression line, yielding an apatite U-Pb lower intercept age of 1218 ± 8 Ma. The large MSWD value implies that multiple age populations likely exist in the sample and a single regression is not appropriate. However, the insufficient number of analysed grains hinders the identification of age populations and more detailed age calculations. Therefore, this age should only be used as a rough guide at this stage.

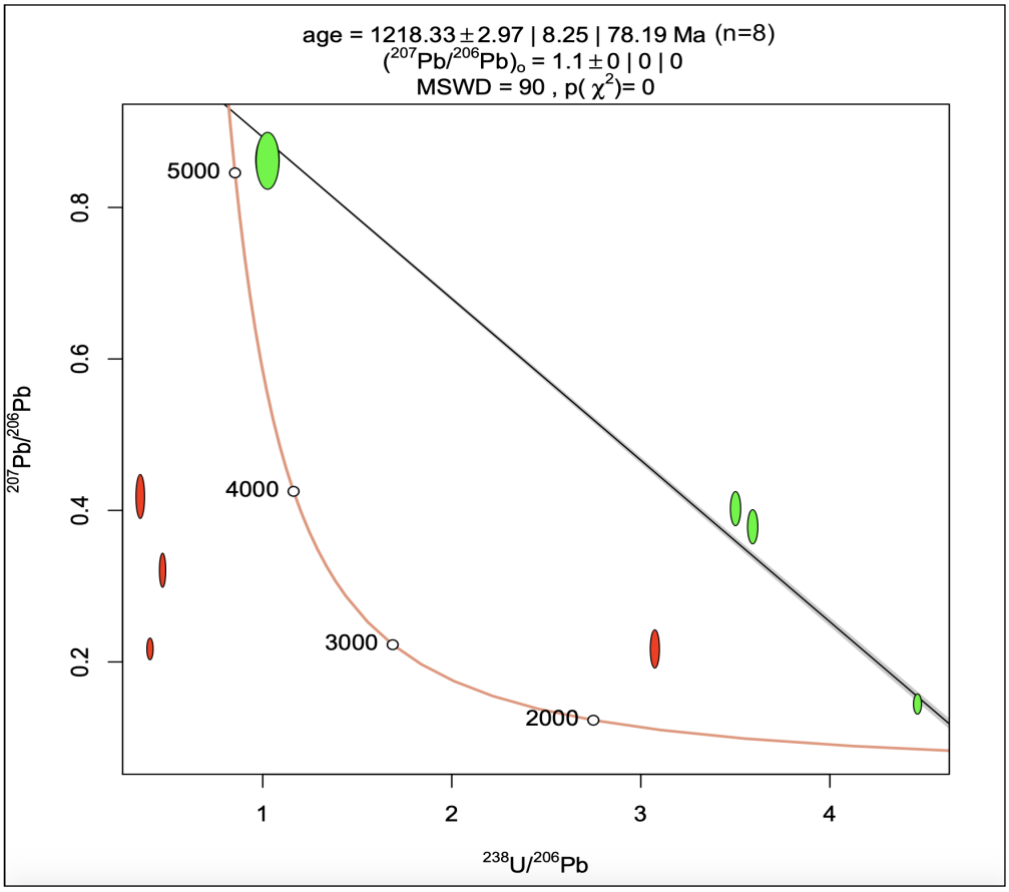

Figure 9: Terra-Wasserburg Concordia plots of all apatite U-Pb results from the BR05DD01 well. Each ellipse plots shows 2σ error for individual grains. (Isoplot R; Vermeesch, 2018)

[4.3] Apatite Fission Track

[4.3.1] Data Accuracy

Each analysed grain of AFT ages is calibrated using Durango apatite standards of known age (Vermeesch, 2017). The weighted mean AFT age of four Durango apatite standard in this thesis is 31.7 ± 4.8 Ma which is within the error of 31.44 ± 0.18 Ma by McDowell *et al.* (2005). This suggests that the LA-ICP-MS and fission track counting is reliable.

[4.3.2] Radial Plot

Figure 10 shows a radial plot of single-grain apatite fission track (AFT) ages to test for multiple age populations. The AFT central age for the entire data-set was calculated at 176 ± 26 Ma. However, given the significant single-grain dispersion (>39%) and the χ^2 probability below the threshold of 5%, multiple age components may be present (Green, 1981). Two age peaks were statistically derived in the plot, calculated at 114 ± 11 Ma and 223 ± 13 Ma. Grains with higher Uranium concentrations are associated with the youngest trend in the plot, suggesting that there may be a radiation damage control on the annealing properties (Hendriks and Redfield, 2005).

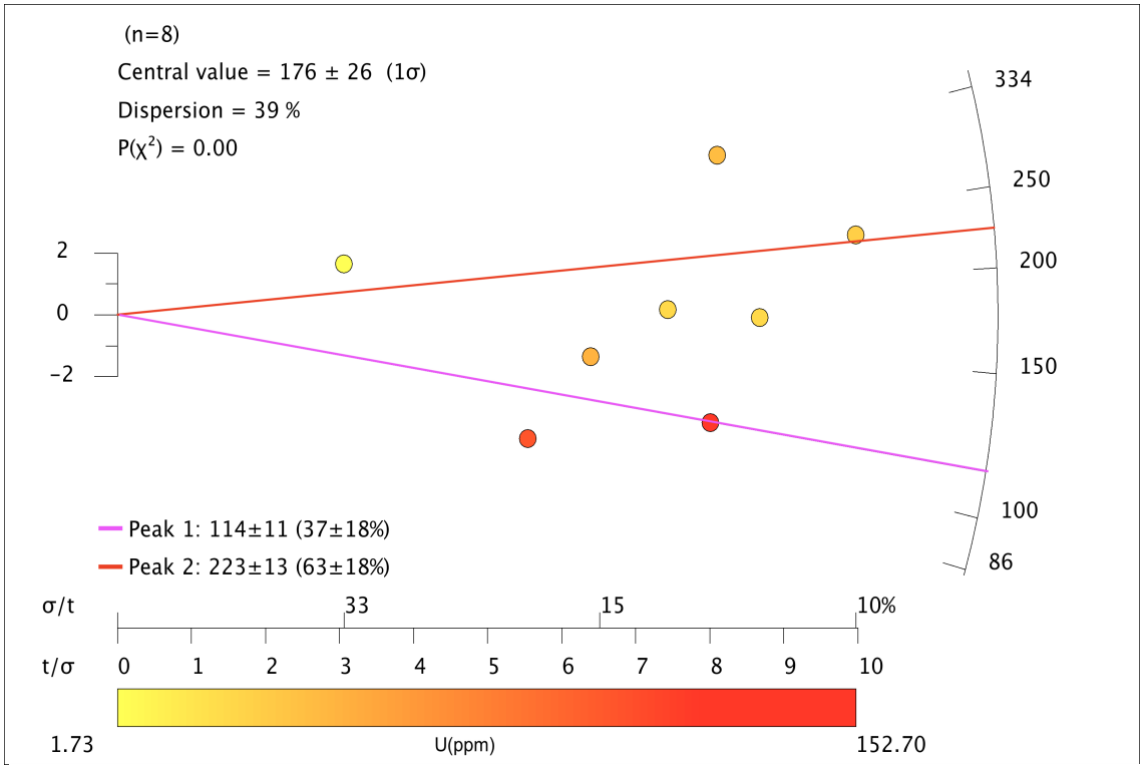

Figure 10: Radial plots of all apatite grains from the BR05DD01 well, plotting precision (t/σ) vs single grain AFT ages. Colour of the symbols signify the uranium concentration in each grain. (RadialPlotter; Vermeesch 2009, 2017)

Sample ID	Formation	Depth (m)	^{238}U±1σ (ppm)	T (Ma)	SD t (Ma)	P(χ^2)	P1±1σ (Ma)	P2±1σ (Ma)
B3(i)-2	Areyonga Formation	507.5 - 509.5	48.8±3.1	142.69	22.31	0.00	114±11	223±13
B3(ii)-4			152.7±8.9	114.08	14.25			
B3(ii)-7			25.8±1.3	174.54	20.12			
B3(ii)-8			25.0±1.5	180.63	24.30			
B12(i)-16		523.8 - 525.8	1.7±0.14	304.05	99.25			
B12(ii)-5			32.5±1.8	228.30	22.90			
B12(ii)-9			42.4±3.1	333.50	41.18			
B12(ii)-10			106.0±11	85.73	15.46			

Table 3: Summary of AFT results obtained from the BR05DD01 well.

[5] DISCUSSIONS

[5.1] Constraints on deposition

The Pioneer Sandstone has a maximum depositional age of 624 ± 12 Ma. It is lateral equivalent and correlated with the Elatina glacial rocks of Adelaide Fold Belt, with a maximum and minimum age limits of 640 and 580 Ma (Lindsay, 1993). It has also been correlated with the 651 ± 87 Ma glacial successions of Georgina Basin, diamictite member of Mt Doreen Formation in the Ngalia Basin and Chambers Bluff Tillite in Officer Basin (Freeman et al., 1991).

The maximum depositional age for the Winnall Group is 491 ± 10 Ma, however, there isn't a definite age that defines this group. Wells *et al* (1970) considered it to be correlative to the Pertatataka Formation but Haines *et al* (2010) proposed the Winnall beds to post-date the Pertatataka Formation. Eventually, Donnellan and Normington (2017) redefined the Winnall Group to include the Pertatataka Formation, 635 – 582 Ma. However, this age is older than the maximum age constraint of the Winnall Group.

The Mt Currie Conglomerate has a maximum depositional age of 685 ± 16 Ma and is inconsistent with geological interpretations by Haines *et al* (2012), entirely early Cambrian. This might possibly be due to contamination. Maximum depositional age in the Stairway Sandstone is 480 ± 9 Ma, which is correlative to the ages discovered by Zhang *et al* (2003) and Maidment (2005), period of Dariwillian to eatly Gisbornian with large number of zircons with age in range 650 – 500 Ma.

The maximum depositional age for the Carmichael Sandstone is 455 ± 13 Ma, though it lacks definitive age evidence for the succession. Edgoose (2013) proposed that it is deposited in the Late Ordovician (460 – 440 Ma), which corresponds to this maximum depositional age. The Mereenie Sandstone has a maximum depositional age

of 554 ± 10 Ma. Due to it being one of the most widespread units of the basin, it is difficult constraining the maximum and minimum age deposition of this formation. Only constraints are through the overlying and underlying units; between the Late Ordovician and Early Devonian (460 – 393 Ma).

[5.2] Kernel Distribution Estimate (KDE) and Multidimensional Scaling (MDS)

In this study, both KDE and MDS plots are used to minimize inaccuracy caused by the MDS and enhance spatial analysis beyond the KDE method. Published igneous zircon U-Pb ages (LA-ICP-MS and SHRIMP data) from potential source regions surrounding the Amadeus Basin were collected and used in the KDE and MDS analysis. These potential source areas are the Paterson Orogen, Tanami Region and Arunta Region in the northwest and north, and the Musgrave Province in the south (Figure 11) (Yang, 2018).

In Figures 11 and 13, the nineteen outcrop samples have been grouped according to the formation that they were sourced from and plotted against the potential source areas, identified above. All formations share similar prominent peak at ca. 1090 – 1165 Ma and a less prominent peak at ca. 1580 – 1800 Ma. Only four formations from all six illustrate an early stage peak at ca. 560 – 650 Ma. The middle prominent peak in all formations coincide with the Musgrave Province and Paterson Orogen as possible source areas whereas the later peak correlates with Arunta and Tanami regions which are both situated in the northern region (Figure 11, 12). The earliest peaks correlate with the zircon U-Pb ages in the possible source area of Paterson Orogen (Figure 11). Conversely, the older zircons are conceivably sourced from the northern regions (Arunta and Tanami).

In the MDS plot, the lowest similarity values are plotted farthest to one another, solid line indicate closest and dashed line indicates second-closest neighbours (Figure 13). The MDS graph suggests that both the Paterson Province and Musgrave Province are closely related to all formations analysed in the basin since they are closely clustered. This result agrees with the KDE graphs but rejects the similarities with the Arunta and Tanami regions. The dissimilarity is likely related to the low amount of old detrital zircons analysed in order to correlate them with the older possible source regions (Arunta and Tanami).

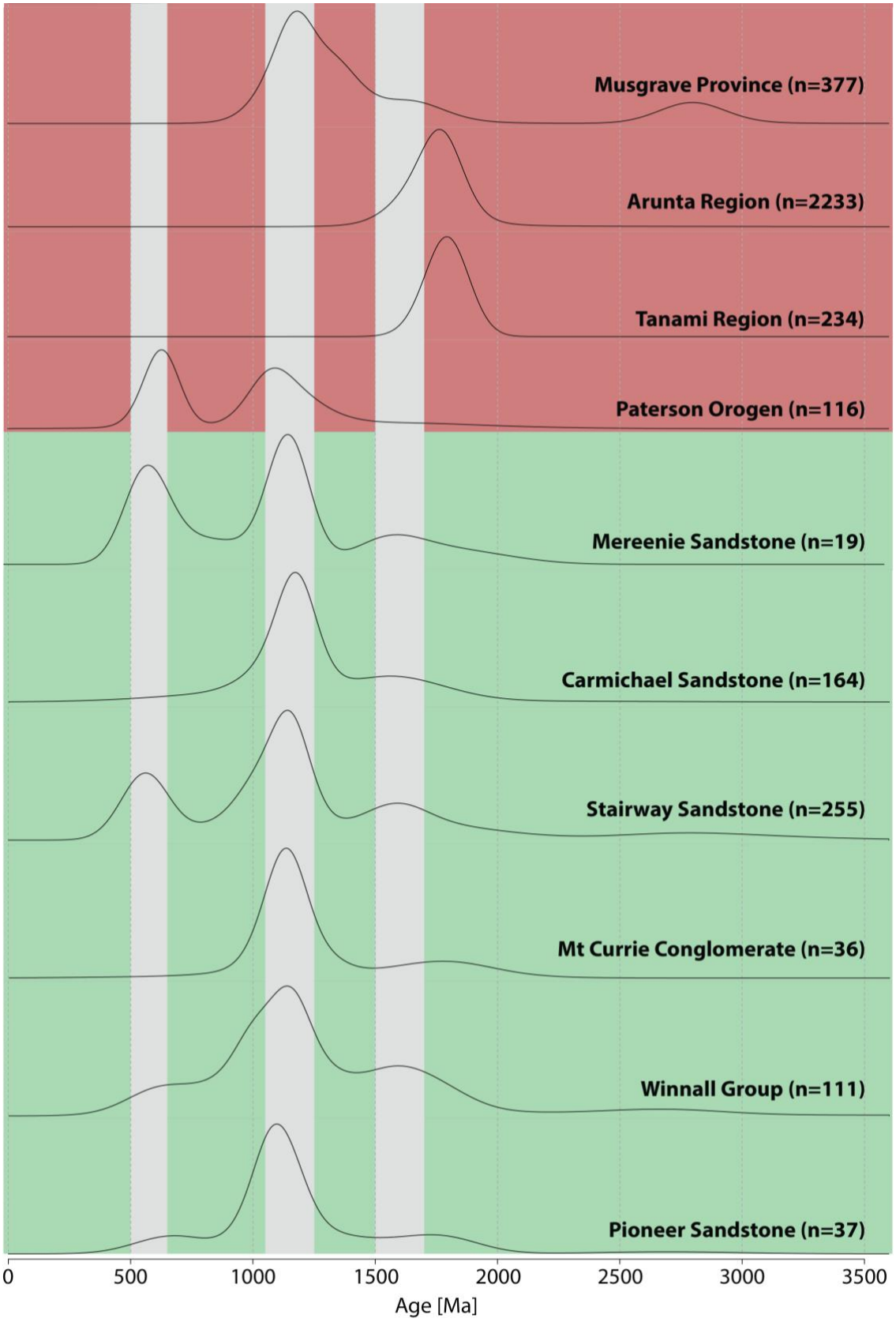

Figure 11: Kernel density estimation (KDE) plots of zircon ages from potential source areas and detrital zircon ages from each analysed formation. Grey bands highlight equivalent ranges.

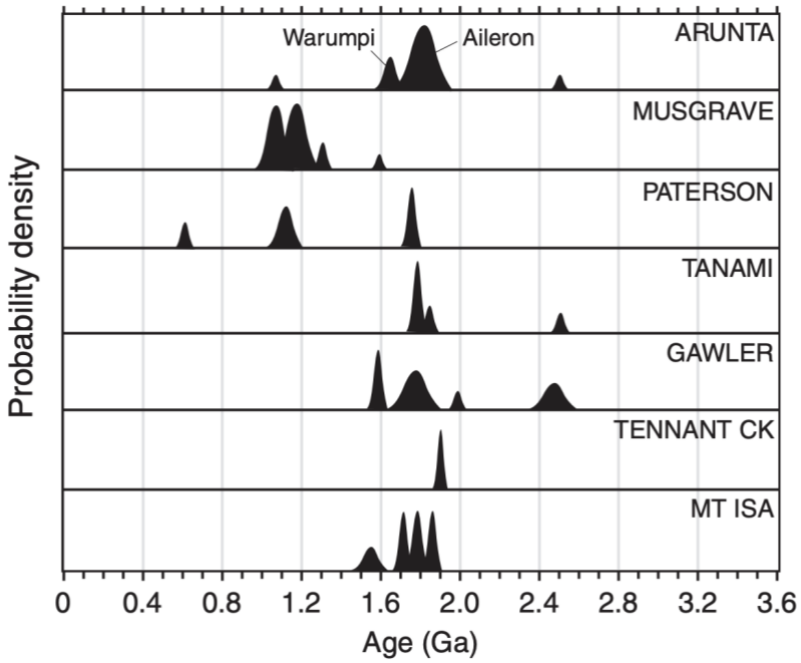

Figure 12: Zircon probability density plots for potential source areas in central Australia. The compilations of zircon U-Pb ages are from Pell et al., (1997) and Camacho et al., (2002).

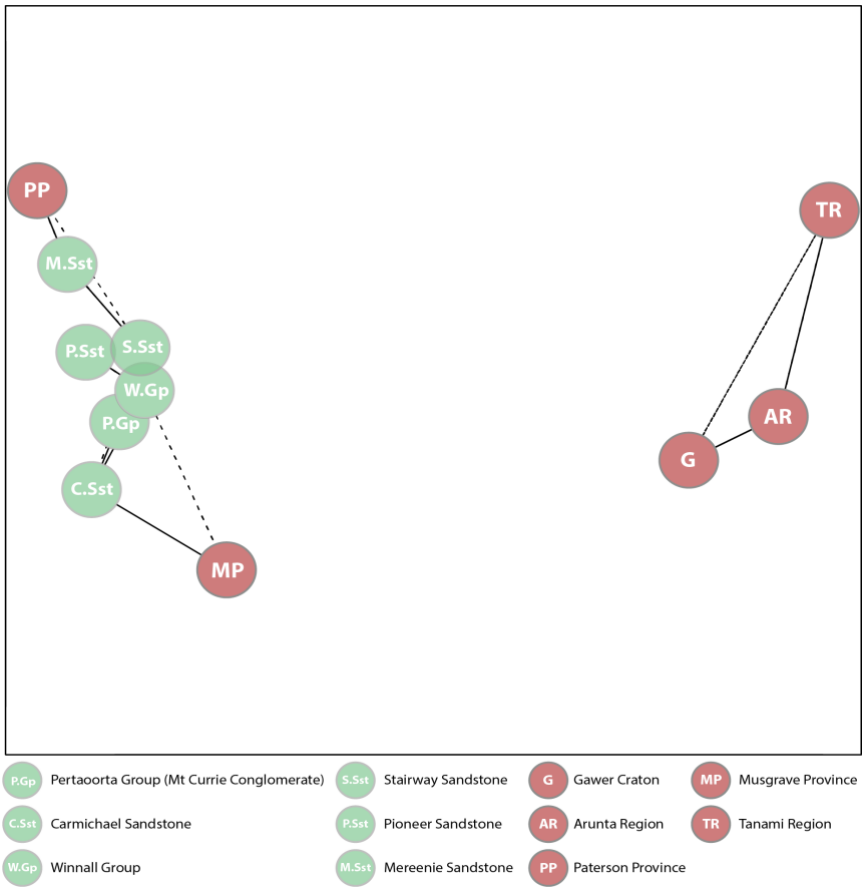

Figure 13: Multidimensional scaling (MDS) plot for the analysed zircon samples (green) and possible source regions (red). Samples with lowest similarity values are plotted farthest to one another; solid line indicate closest and dashed line indicates second-closest neighbours.

[5.3] Provenance analysis

The Neoproterozoic Pioneer Sandstone shows a prominent peak at ca. 1096 Ma which is likely derived largely from rocks of the ca. 1090 – 1040 Ma Giles Event that have been grouped into the Warakurna Supersuite in the central-western Musgrave Province (Howard et al., 2011; Glikson et al., 1996). The zircons could also possibly be sourced from the similar age ca. 1090 – 1040 Ma Tjauwata Group situated between the Petermann Ranges and Blood Range in the northern Musgrave Province. This formation with an earlier minor peak at ca. 646 Ma could be sourced from the related to metamorphism and pegmatites coeval with the ca. 650 – 611 Ma Miles Orogeny in the Rudall Province, exposed about ~600 km northwest of the outcropping Musgrave Region (Figure 3) (Dunphy and McNaughton, 1998; Bagas, 2004). The final third peak illustrated at ca. 1740 Ma coincides with the compilations of zircon U-Pb ages, mainly derived from the Aileron Province (Figure 11 and 12). This could be related with the Strangways Event occurring in the eastern and southeastern Aileron Province.

The Winnall Group unconformably overlain by Mt Currie Conglomerate is likely to correlate with Arumbera Sandstone in the upper succession and Pertatataka Formation in the lower succession (Haines et al., 2010, 2012). Unlike the Pioneer Sandstone, the Winnall Group has a slightly older prominent peak at ca. 1148 Ma but also showing a dominant source from the Musgrave Province (Figure 11 and 12). Younger peak at ca. 624 Ma is similar to the Pioneer Sandstone, which means the detrital zircons could also be sourced from the ca. 650 – 611 Ma Miles Orogeny in Rudall Province. However, the later peak at ca. 1584 Ma could indicate material derived from the Chewings Orogeny in the Arunta Region. Another possible source of the older

aged zircon grains is from the gneisses such as the Musgravian gneiss in the Musgrave province with igneous crystallization age of 1600 – 1540 Ma.

Sweet and Crick (1992) suggested that the Early Cambrian Mt Currie Conglomerate correlates with the Mutitjulu Arkose, which was previously and informally named 'Uluru arkose'. Forman (1965), Wells *et al* (1970) and Sweet and Crick (1992) proposed that this stratigraphic unit is a proximal foreland succession, deposited in a piedmont setting resulted from the uplifted Musgrave Province and overlying Neoproterozoic units of the Amadeus Basin during the Petermann Orogeny. Variations from sedimentary rocks to volcanic rocks to granite in the composition of Mt Currie Conglomerate reflects the exposure of older rocks of the Musgrave Province at that time. The prominent peak shown at ca. 1134 Ma suggest that the Musgrave Complex is the primary detrital source since the majority of ages for the Musgrave Complex, prior to the Petermann Orogeny, are ca. 1200 – 1050 Ma. The zircons could be derived from the Pitjantjatjara Supersuite. A less prominent peak illustrated at ca. 1791 Ma correlates with the 1810 – 1790 Ma Stafford Event that affected extensive areas in the Aileron Province (Figure 11 and 12). Therefore, these older zircons could perhaps be recycled detritus originally from the Arunta Region and transported via eroded Supersequence 1-3 Amadeus Basin sediments.

The Early Ordovician Stairway Sandstone shows a young peak at ca. 560 Ma and this correlates with the detrital zircons in Paterson Province (Figure 11 and 12). This could possibly be sourced during the ca. 550 Ma Paterson Orogeny which is linked to the Petermann Orogeny, Paterson-Petermann Orogen (Figure 3). The exhumation during the ca. 550 Ma Paterson-Petermann Orogen may have deposited detrital zircons of the young Telfer granite (625 – 500 Ma) from the Paterson Orogen (Bagas, 2004).

The correlation of this young peak with the Paterson Province is illustrated in the compiled possible source regions (Figure 11 and 12). The prominent peak at ca. 1141 Ma, which is contemporaneous with the widespread ca. 1130 – 1220 Pitjantjatjara Supersuite granites during the Musgrave Orogeny. The small cluster of zircons at ca. 1580 – 1610 Ma is consistent with the age of the Chewings Orogeny sourcing from both the Aileron and Warumpi Province.

The poorly exposed Late Ordovician Carmichael Sandstone, however, only shows two later peaks with an absence of the early peak (Figure 8). This non-existent peak can be due to the Musgrave Province being covered and could therefore not supply detritus to the Amadeus Basin. In addition, the initiation of major compressional Rodingan Event during ca. 450 – 440 Ma coincides with the stratigraphic age of the Carmichael Sandstone. This compressional event may have influenced the Amadeus Basin, which may have acted as a foreland basin and buried the Musgrave Province during this period (Walsh, 2015). Since the Musgrave Province has been buried, the only source could have been from the northern part (e.g. Amadeus Basin) deposited during the Rodingan Event, therefore, the prominent peak illustrated at ca. 1163 Ma corresponds to the Teapot Event in southern Arunta Province and the older peak at ca. 1554 Ma agrees to the age of Chewings Orogeny in Arunta Region, similarly to the Stairway Sandstone.

The Silurian-Devonian Mereenie Sandstone is one of the most widespread units in the Amadeus Basin (Owen in Kennard and Nicoll, 1986). The age spectrum of this unit illustrates two prominent peaks at ca. 582 and 1156 Ma. Well *et al* (1970) interpreted similar zircon age constraints in relation to the reworking of underlying Cambro-Ordovician successions resulted from the uplift in the northeastern part of the

basin during Rodingan Movement. The return presence of early peak in the Mereenie Sandstone can be due to the intensive Alice Springs Orogeny during this period, which interacted with the Musgrave Province, exhuming the province and exposing it once again. Furthermore, the AFT ages across Musgrave Province and southern Amadeus Basin indicate exhumation and cooling in latter stages of the Alice Springs Orogeny (Tingate, 1990). The excellent similarity of the early zircon age peaks with the Stairway Sandstone could also suggest that the Paterson-Petermann Orogen could have been the source, sourcing young detrital zircons from the Paterson Orogen. The second prominent zircon age peak at ca. 1156 Ma correlates well with the widespread ca. 1150 – 1220 Pitjantjatjara Supersuite granites, which formed during extension and ultra-high temperature conditions in the Musgrave Orogeny. The third less prominent peak shown at ca. 1595 Ma associates with the ages of Chewings Orogeny, similarly to both later peaks of Carmichael and Stairway sandstones.

[5.4] Apatite thermal history

In the AUPb plot, can only be concluded that it does not pass the P(χ^2)-test which signifies multiple AFT age populations within the data. From all the apatite grains analysed, it can be observed that the apatite fission track ages are younger than the stratigraphic age (Areyonga Formation; ca. 720 – 660 Ma). The apatite grains have been heated above >120ºC, passing the AFT closure temperature, after they were deposited in the basin (fully reset). Therefore, the AFT ages cannot help constraining the provenance and maximum possible depositional age of the rock since they have been thermally reset. However, the AFT ages give an indication of the timing of burial and subsequent cooling in the basin.

The AFT results do not pass the P(χ^2)-test and a great dispersion within the data, also signifying multiple AFT age populations. Given that we ruled out a relation of multiple populations with a different provenance, the identified two populations of ~223 Ma and ~114 Ma must reflect different parts of a common thermal history. Given the observed compositional differences between the two populations (i.e. uranium concentrations), the different ages are interpreted in terms of different temperatures to which the fission tracks in high versus low U grains anneal (Hendriks and Redfield, 2005). The thermal history cannot be modelled in this thesis due to the absence of confined-track lengths in all apatite grains. However, we can speculate on the thermal history, using the significant single-age dispersion and the identified age populations. Two possible models would fit the AFT data; (a) a burial history that started at ~223 Ma and reached a maximum temperature in the Cretaceous, before the sample cooled below 60 – 80^{o}C at ~114 Ma, or (b) slow steady cooling after burial above 120^{o}C, for a long period since the Triassic where different temperature intervals were crossed corresponding to the peak ages. Unfortunately, there are insufficient data to confirm one of these models, however, the absence of Cretaceous deformation would support model (b).

[6] CONCLUSIONS

New detrital zircon and apatite data presented in this research provides constraints on the provenance and thermal evolution of the southern Amadeus Basin. Kernel Distribution Estimate (KDE) and Multidimensional Scaling (MDS) were used to identify the spatial and temporal provenance of the analysed samples. The apatite fission track data were used to speculate on the post-depositional thermal history of the basin. The main conclusions in this research are:

(1) The major compressional Rodingan Event (ca. 450 – 440 Ma) associated with the Alice Springs Orogeny may have influenced the Amadeus Basin, which may have acted as a foreland basin which resulted in the burial of Musgrave Province. Therefore, the Late Ordovician Carmichael Sandstone exhibits provenance from the Arunta Region.

(2) Detrital zircon U-Pb age data (ca. 1156 – 1086 Ma) from the Mereenie, Stairway, Pioneer Sandstones, Mt Currie Conglomerate (Pertaoorta Group) and Winnall Groups, all show a consistent provenance dominated by Musgrave Region.

(3) Early zircon U-Pb age peaks (ca. 646 and 624 Ma) in Pioneer Sandstone and Winnall Group are sourced from the Miles Orogeny in Rudall Province, as well as, early peaks (ca. 560 and 582 Ma) in Stairway and Mereenie Sandstones are sourced by the Paterson Orogeny, which are both orogenies are linked to the Paterson-Petermann Orogen.

(4) The later age peaks (ca. 1595 – 1584 Ma) in Mereenie, Stairway Sandstone and Winnall Group are sourced from the Chewings Orogeny in the Arunta Region and minor contributions inferred to be from the Musgravian gneiss in

the Musgrave Province. Older age peaks (ca. 1740 and 1791 Ma) in Pioneer Sandstone and Mt Currie Conglomerate interpreted to have been sourced from the Stafford and Strangways Event in the Arunta Region.

(5) Apatite grains have been heated above AFT closure temperature (120^{o}C) after being deposited in the basin and, therefore, don't provide provenance information.

(6) The AFT data can be decomposed into 2 AFT age populations with respect to varying U concentrations. The ~223 Ma and ~114 Ma age populations likely represent an extensive thermal history in the apatite partial annealing zone.

[7] ACKNOWLEDGMENTS

I would like to thank my primary supervisor Dr. Stijn Glorie, secondary supervisor Prof. Alan Collins, PhD student Angus Nixon and Dr. Morgan Blades for all their assistance and being extremely supportive throughout the year. I would also like to acknowledge the contribution of Sandra Menpes and Mattilda Sheridan from Santos for providing the samples in this project. Finally, I would like to thank Sarah Gilbert and David Kelsey from Adelaide Microscopy for their assistance and support during analysis of samples.

[8] REFERENCES

AITKEN, A.R.A., BETTS, P.G., AILLERES, L., 2009. The architecture, kinematics, and lithospheric processes of a compressional intraplate orogen occurring under Gondwana assembly: the Petermann Orogeny, central Australia. Lithosphere 1, 343–357.

AMBROSE, G.J., 2006. Northern Territory of Australia, Onshore hydrocarbon potential 2006. Northern Territory Geological Survey Record 2006-003.

BAGAS, L., 2004. Proterozoic evolution and tectonic setting of the northwest Paterson Orogen, Western Australia. Precambrian Research 128, 475–496.

BRADSHAW, J.D. & EVANS, P.R., 1988. Palaeozoic tectonics, Amadeus Basin, central Australia. APEA Journal 28, 267–282.

BUICK, I.S., HAND, M., WILLIAMS, I.S., MAWBY, J., MILLER, J.A., NICOLL, R.S., 2005. Detrital zircon provenance constraints on the evolution of the Harts Range Metamorphic Complex (central Australia): links to the Centralian Superbasin. Journal of the Geological Society, London 162, 777–787.

CAMACHO, A., HENSEN, B.J. & ARMSTRONG, R., 2002. Isotopic test of a thermally driven intraplate orogenic model, Australia. *Geology* 30, 887 – 890.

CAMACHO, A., MCDOUGALL, I., 2000. Intracratonic, strike-slip partitioned transpression and the formation of eclogite facies rocks: an example from the Musgrave Province, central Australia. Tectonics 19, 978–996.

CHEW, D.M., PETRUS, J.A., KAMBER, B.S., 2014. U-Pb LA–ICPMS dating using accessory mineral standards with variable common Pb. Chem. Geol. 363, 185–199.

CLOSE, D.F., 2013. Chapter 21: Musgrave Province. In: AHMAD, M., MUNSON, T.J. (Eds.), Geology and Mineral Resources of the Northern Territory. Northern Territory Geological Survey, Special Publication 5, pp. 21.1–21.24.

COOK, P.J., 1972. Sedimentological studies on the Stairway Sandstone of central Australia. Bureau of Mineral Resources, Australia, Bulletin 95.

CZARNOTA, K., GERNER, E., MAIDMENT, D.W., MEIXNER, A., BAGAS, L., 2009. Paterson area 1:250 000-scale solid geology interpretation and depth to basement model — explanatory notes. Geoscience Australia, Record 2009/16.

DICKINSON, W.R., GEHRELS, G.E., 2009. Use of U-Pb ages of detrital zircons to infer maximum depositional ages of strata: a test against a Colorado Plateau Mesozoic database. Earth Planet. Sci. Lett. 288 (1), 115-125

DONNELLAN, N. & NORMINGTON, V. 2017. Towards a revised stratigraphy for the Neoproterozoic and probable early Cambrian in the central Amadeus Basin, Northern Territory. In: *AGES 2017 Proceedings*. [online] Alice Springs: NT Geological Survey, pp.80-85. Available at: https://geoscience.nt.gov.au/gemis/ntgsjspui/bitstream/1/85119/3/DonnellanAGES2017_paper.pdf [Accessed 1 Oct. 2018].

DUNPHY, J.M. & MCNAUGHTON, N.J., 1998. Geochronology of the Telfer granitoids: zircon and titanite U–Pb SHRIMP data. Geological Society of Australia Abstracts, 49, 127.

DYSON, I.A. & MARSHALL, T.R., 2007. Neoproterozoic salt nappe complexes and salt withdrawal mini-basins in the Amadeus Basin: in MUNSON T.J. and AMBROSE G.J. (editors) Proceedings of the Central Australian Basins Symposium, Alice Springs 16 – 18 August 2005. *Northern Territory Geological Survey, Special Publication 2*, 108 – 118.

EDGOOSE, C.J., 2013a. Chapter 23: Amadeus Basin. In: AHMAD, M., MUNSON, T.J. (Eds.), Geology and Mineral Resources of the Northern Territory. Northern Territory Geological Survey, Special Publication 5, pp. 23.1–23.70.

EDGOOSE, C.J., 2013b. Chapter 24: Ngalia Basin. In: AHMAD, M., MUNSON, T.J. (Eds.), Geology and Mineral Resources of the Northern Territory. Northern Territory Geological Survey, Special Publication 5, pp. 24.1–24.24.

EDGOOSE, C.J., SCRIMGEOUR, I.R. & CLOSE, D.F., 2004. Geology of the Musgrave Block, Northern Territory. Northern Territory Geological Survey, Report 15.

FLÖTTMANN, T., HAND, M., CLOSE, D.F., EDGOOSE C.J. & SCRIMGEOUR, I.R., 2004. Thrust tectonic styles of the intracratonic Alice Springs and Petermann orogenies, central Australia: in MCCLAY, K.R., (editor) *'Thrust tectonics and hydrocarbon systems'. American Association of Petroleum Geologists, Memoir* 82, 538 – 557.

FREEMAN, M.J., OAKS, R.Q., & SHAW, R.D., 1991. Stratigraphy of the Late Proterozoic Gaylad Sandstone, northeastern Amadeus Basin, and recognition of an underlying regional unconformity: in Korsch RJ and Kennard JM (editors) 'Geological and geophysical studies in the Amadeus Basin, central Australia'. Bureau of Mineral
Resources, Australia, Bulletin 236, 137-154.

FORMAN, D.J., 1965. Ayers Rock, Northern Territory, 1:250 000 geological map series explanatory notes, SG 52-08. Bureau of Mineral Resources, Australia, Canberra.

GEHRELS, G., 2014. Detrital zircon U-Pb geochronology applied to tectonics. Annu. Rev. Earth Planet. Sci. 42, 127-149.

GIBSON, H., DUDDY, I., AMBROSE, G., and MARSHALL, T., 2005. Regional perspective on new and reviewed thermal history data from central Australian basins. In Proceedings of The Central Australian Basins Symposium, (Alice Springs: Northern Territory Geological Survey).

GREEN, P.F., 1981: A new look at statistics in fission track dating. Nuclear Tracks and Radiation Measurements 5, 77–86.

GREGORY, C.J., BUICK, I.S., HERMANN, J., RUBATTO, D., 2009. Mineral-scale trace element and U– Th–Pb age constraints on metamorphism and melting during the Petermann Orogeny (central Australia). Journal of Petrology 50, 251–287.

HAINES, P.W., HAND, M., & SANDIFORD, M., 2001. Palaeozoic synorogenic sedimentation in central and Northern Australia: a review of distribution and timing with implications for the evolution of intracontinental orogens. Australian Journal of Earth Sciences 48, 911 – 928.

HAINES, P.W., ALLEN, H.J., & Grey, K., 2010. Reassessment of the geology and exploration potential of the Western Australian Amadeus Basin. Geological Survey of Western Australia, Extended Abstracts.

HAINES, P.W., ALLEN, H.J., GREY, K. & EDGOOSE, C.J., 2012. The western Amadeus Basin: revised stratigraphy and correlations: in AMBROSE, G.J. and SCOTT, J. (editors). 'Central Australian Basins Symposium (CABS) III'. Petroleum Exploration Society of Australia, Special Publication.

HAINES, P.W., ALLEN, H.J., WINGATE M.T.D., KIRKLAND, C. & EDGOOSE, C.J., 2012b. Syn-tectonic (Petermann Orogeny) deposition tracked through detrital zircon geochronology, western Amadeus Basin, central Australia. *34th International Geological Congress, Abstracts*, 1091.

HAINES, P.W., KIRKLAND, C.L., WINGATE, M.T.D., ALLEN, H., BELOUSOVA, E.A & GRÉAU, Y. 2016. Tracking sediment dispersal during orogenesis: A zircon age and Hf isotope study from the western Amadeus Basin, Australia. *Gondwana Research*, 37, pp.324-347.

HAINES, P.W. & WINGATE, M.T.D., 2007. Fingerprinting reservoir sandstone provenance in the Canning Basin using detrital zircons. Western Australia Geological Survey, Annual Review 2005–06, in press.

HENDRIKS, B. & REDFIELD, T. 2005. Apatite fission track and (U-Th)/He data from Fennoscandia: An example of underestimation of fission track annealing in apatite. *Earth And Planetary Science Letters* 236, 443-458.

HOWARD, K.E., HAND, M., BAROVICH, K.M., REID, A., WADE, B.P., BELOUSOVA, E.A., 2009. Detrital zircon ages: Improving interpretation via Nd and Hf isotopic data. Chemical Geology 262, 277-292.

HOWARD, H.M., SMITHIES, R.H., KIRKLAND, C.L., KELSEY, D.E., AITKEN, A., WINGATE, M.T.D., QUENTIN DE GROMARD, R., SPAGGIARI, C.V., MAIER, W.D., 2015. The burning heart — the Proterozoic geology and geological evolution of the west Musgrave Region, central Australia. Gondwana Research 27, 64–94.

JACKSON, S.E., PEARSON, N.J., GRIFFIN, W.L., BELOUSOVA, E.A., 2004. The application of laser-ablation-inductively coupled plasma-mass spectrometry to in situ U–Pb zircon geochronology. Chem. Geol., 211, pp. 47-69

JONES, B.G., 1972. Upper Devonian to Lower Carboniferous stratigraphy of the Pertnjara Group, Amadeus Basin, central Australia. Journal of the Geological Society of Australia 19(2), 229 – 249.

KENNARD, J.M. & NICOLL R.S., 1986. Late Proterozoic and early Palaeozoic depositional facies of the northern Amadeus Basin, central Australia. Sediments Down-under. 12th International Sedimentological Congress, Canberra, *Australia, 24 – 30 August 1986. Field Excursion* 25B. Bureau of Mineral Resources, Canberra.

KENNERDY, M., 1993. The Undoolya Sequence: Late Proterozoic salt influenced deposition, Amadeus Basin, central Australia. *Australian Journal of Earth Sciences* 40, 217 – 228.

KORSCH, R.J. & KENNARD, J.M., (editors), 1991. 'Geological and geophysical studies in the Amadeus Basin, central Australia'. Bureau of Mineral Resources, Australia, Bulletin 236.

LINDSAY, J.F., 1989. Depositional controls on glacial facies associations in a basinal setting, Late Proterozoic, Amadeus Basin, central Australia. Palaeogeography, Palaeoclimatology, Palaeoecology 73, 205 – 232.

LINDSAY, J.F. (editor), 1993. Geological atlas of the Amadeus Basin. Bureau of Mineral Resources, Australia, Canberra.

LUDWIG, K.R., 1999. Using Isoplot/Ex, Version 2.01: a geochronological toolkit for Microsoft Excel. Berkeley Geochronology Center Special Publication, No. 1a: 47.

MABOKO, M.A.H., MCDOUGALL, I., ZEITLER, P.K. & WILLIAMS, I.S., 1992. Geochronological evidence for ~ 530-550 Ma juxtaposition of two Proterozoic metamorphic terranes in the Musgrave Ranges, central Australia. Aust. J. Earth Sci., 39: 457471.

MAIDMENT, D.W., 2005. *Palaeozoic high-grade metamorphism within the Centralian Superbasin, Harts Range region, central Australia*. PhD thesis, Research School of Earth Sciences, Australian National University, Canberra.

MAIDMENT, D.W., WILLIAMS, I.S. & HAND, M., 2007. Testing longterm patterns of basin sedimentation by detrital zircon geochronology, Centralian Superbasin, Australia. *Basin Research 19*, 335 – 360.

MCDOWELL, F.W., MCINTOSH, W.C., FARLEY, K.A., 2005. A precise 40Ar–39Ar reference age for the Durango apatite (U–Th)/He and fission-track dating standard. Chem. Geol. 214 (3–4), 249–263.

MCLENNAN S.M., HEMMING, S., MCDANIEL D.K., HANSON G.M., 1993. Geochemical approaches to sedimentation, provenance, and tectonics. JOHNSSON, M.J., BASU, A., (Eds.), Processes Controlling the Composition of Clastic Sediments, Geological Society of America Special Papers, vol. 284, pp. 21–40.

MUNSON, T.J., KRUSE, P.D. & AHMAD, M., 2013. Chapter 22: Centralian Superbasin: in AHMAD, M. & MUNSON, T.J. (compilers). 'Geology and mineral resources of the Northern Territory'. Northern Territory Geological Survey, Special Publication 5.

PRIESS, W.V., WALTER, M.R., COATS, R.P. & WELLS, A.T., 1978. Lithological correlations of Adelaidean glaciogenic rocks in parts of the Amadeus, Ngalia and Georgina Basins. BMR Journal of Australian Geology and Geophysics 3, 45 – 53.

RAIMONDO, T., COLLINS, A.S., HAND, M., WALKER-HALLAM, A., SMITHIES, R.H., EVINS, P.M., HOWARD, H.M., 2010. The anatomy of a deep intracontinental orogen. Tectonics 29, 1–31, TC4024.

REINERS, P. W., & EHLERS, T. A., 2005. *Low-temperature thermochronology: techniques, interpretations, and applications* (Vol. 58). Washington, America: The Mineralogy Society of America.

ROE, L.E., 1991. 'Petroleum exploration in the Amadeus Basin'. Bureau of Mineral Resources, Australia, Bulletin 236, 463 – 476.

SCHOENE, B., BOWRING, S.A., 2006. U-Pb systematics of the McClure Mountain syenite: thermochronological constraints on the age of the Ar-40/Ar-39 standard MMhb. Contrib. Miner. Petrol. 151 (5), 615–630.

SCRIMGEOUR, I.R., CLOSE, D.F., 1999. Regional high pressure metamorphism during intracratonic deformation: the Petermann Orogeny, central Australia. Journal of Metamorphic Geology 17, 557–572.

SCRIMGEOUR I.R., CLOSE, D.F. & EDGOOSE, C.J., 1999. Petermann Ranges, Northern Territory (Second Edition). 1:250 000 geological map series explanatory notes, SG 52-07. Northern Territory Geological Survey, Darwin.

SHAW, R.D., 1991. The tectonic development of the Amadeus Basin, central Australia: in Korsch RJ and Kennard JM (editors) 'Geological and geophysical studies in the Amadeus Basin, central Australia'. Bureau of Mineral Resources, Australia, Bulletin 236, 429 – 462.

SHAW, R.D., KORSCH, R.J., WRIGHT, C. & GOLEBY, B.R., 1991. Seismic interpretation and thrust tectonics of the Amadeus Basin, along the BMR regional seismic line: in Korsch RJ and Kennard JM (editors) 'Geological and geophysical studies in the Amadeus Basin, central Australia'. Bureau of Mineral Resources, Australia, Bulletin 236, 385 – 408.

SLÁMA, J., KOSLER, J., CONDON, D.J., CROWLEY, J.L., GERDES, A., HANCHAR, J.M., HORSTWOOD, M.S.A., MORRIS, G.A., NASDALA, L., NORBERG, N., SCHALTEGGER, U., SCHOENE, B., TUBRETT, M.N., WHITEHOUSE, M.J., 2008. Plesovice zircon – a new natural reference material for U-Pb and Hf isotopic microanalysis. Chemical Geology 249, 1-35.

SPENCER, C., KIRKLAND, C. and TAYLOR, R. 2016. Strategies towards statistically robust interpretations of in situ U–Pb zircon geochronology. *Geoscience Frontiers*, 7(4), pp.581-589.

SWEET, I.P., STEWART, A.J. & CRICK, I.H., 2012. Uluru and Kata Tjuta: a geological guide. Geoscience Australia, Canberra.

SWEET, I.P. & CRICK, I.H., 1992. Uluru and Kata Tjuta: a geological history. Australian Geological Survey Organisation, Canberra.

TINGATE, P., 1990. Apatite fission track studies from the Amadeus Basin, central Australia. PhD Thesis, Department of Geology, University of Melbourne, Melbourne.

TINGATE, P., 1991. Apatite fission track analysis of the Pacoota and Stairway Sandstones, Amadeus Basin, central Australia: in Korsch RJ and Kennard JM (editors) 'Geological and geophysical studies in the Amadeus Basin, central Australia'. Bereau of Mineral Resources, Australia, Bulletin 236, 525-540.

TYLER, I.M., HOCKING, R.M., HAINES, P.W., 2012. Geological evolution of the Kimberley region of Western Australia. Episodes 35, 298–306.

VERMEESCH, P. 2009. RadialPlotter: A Java application for fission track, luminescence and other radial plots. *Radiation Measurements*, *44*(4), 409-410

VERMEESCH, P., 2012. On the visualisation of detrital age distributions. Chemical Geology, v.312-313, 190-194, doi: 10.1016/j.chemgeo.2012.04.021

VERMEESCH, P. 2017. Statistics for LA-ICP-MS based fission track dating. *Chemical Geology*, *456*, 19-27. doi: 10.1016/j.chemgeo.2017.03.002

WALSH, A.K., RAIMONDO, T., KELSEY, D.E., HAND, M., PFITZNER, H.L., CLARK, C., 2012. Duration of high-pressure metamorphism and cooling during the intraplate Petermann Orogeny. Gondwana Research 24, 969–983.

WALTER, M.R. & BAULD, J., 1983. The association of sulphate evaporites, stromatolitic carbonates and glacial sediments: examples from the Proterozoic of Australia and the Cainozoic of Antarctica. Precambrian Research 21, 129 – 148.

WALTER M.R., VEEVERS, J.J., CALVER, C.R. & GREY, K., 1995. Neoproterozoic stratigraphy of the Centralian Superbasin, Australia. Precambrian Research 73, 173 – 195.

WALSH, A., HAND, M., & KELSEY, D. 2015. A metamorphic perspective on foreland flexure during intraplate orogeny: evidence for the involvement of weak lithosphere. *Terra Nova* 27, 329-337.

WAGNER, G.A., VAN DEN HAUTE, P., 1992. Fission Track-Dating. Kluwer Academic Publishers, Dordrecht.

WEBBY, B.D., 1978. History of the Ordovician continental platform shelf margin of Australia, Journal of the Geological Society of Australia, 25:1-2, 41-63, DOI: 10.1080/00167617808729013

WELLMAN, P., 1991. Amadeus Basin, Northern Territory: structure form gravity and magnetic anomalies: in Korsch RJ and Kennard JM (editors) '*Geological and geophysical studies in the Amadeus Basin, central Australia'. Bureau of Mineral Resources, Australia, Bulletin* 236, 33 – 40.

WELLS, A.T., FORMAN, D.J., RANFORD, L.C. & COOK, P.J., 1970. Geology of the Amadeus Basin, Central Australia. Bureau of Mineral Resources, Australia, Bulletin 100.

YANG, B., SMITH, T., COLLINS, A., MUNSON, T., SCHOEMAKER, B., NICHOLLS, D., COX, G., FARKAS, J., & GLORIE, S. 2018. Spatial and temporal variation in detrital zircon age provenance of the hydrocarbon-bearing upper Roper Group, Beetaloo Sub-basin, Northern Territory, Australia. *Precambrian Research* 304, 140-155.

ZHAO, JIANXIN., MCCULLOH, M.T. & BENNETT, V.C., 1992. Sm-Nd and U-Pb zircon isotopic constraints on the provenance of sediments from the Amadeus Basin, central Australia: Evidence for REE fractionation. *Geochimica et Cosmochimica Acta* 56, 921 – 940.

ZHANG JIANHUA, BARNES, C.R., & COOPER, B.J., 2003. Early Late Ordovician conodonts from the Stokes Siltstone, Amadeus Basin, central Australia: in Mawson R and Talent JA (editors) 'Contributions to the Second Australian conodont Symposium (AUSCOS II) held in conjunction with Palaeontology DownUnder – 2000 in Orange, Australia, 3-7 July 2000. Volume dedicated to the memory of Willy Ziegler'. Courier Forschungsinstitut Senckenberg 245, 1-37.

APPENDIX A: OUTCROP SAMPLES

Figure 14: Outcrop Samples of KULGERA; top left: Mereenie Sst, top right: Carmichael Sst, bottom left: Stairway Sst; bottom right: Mt Currie Conglomerate (Pertaoorta Group)

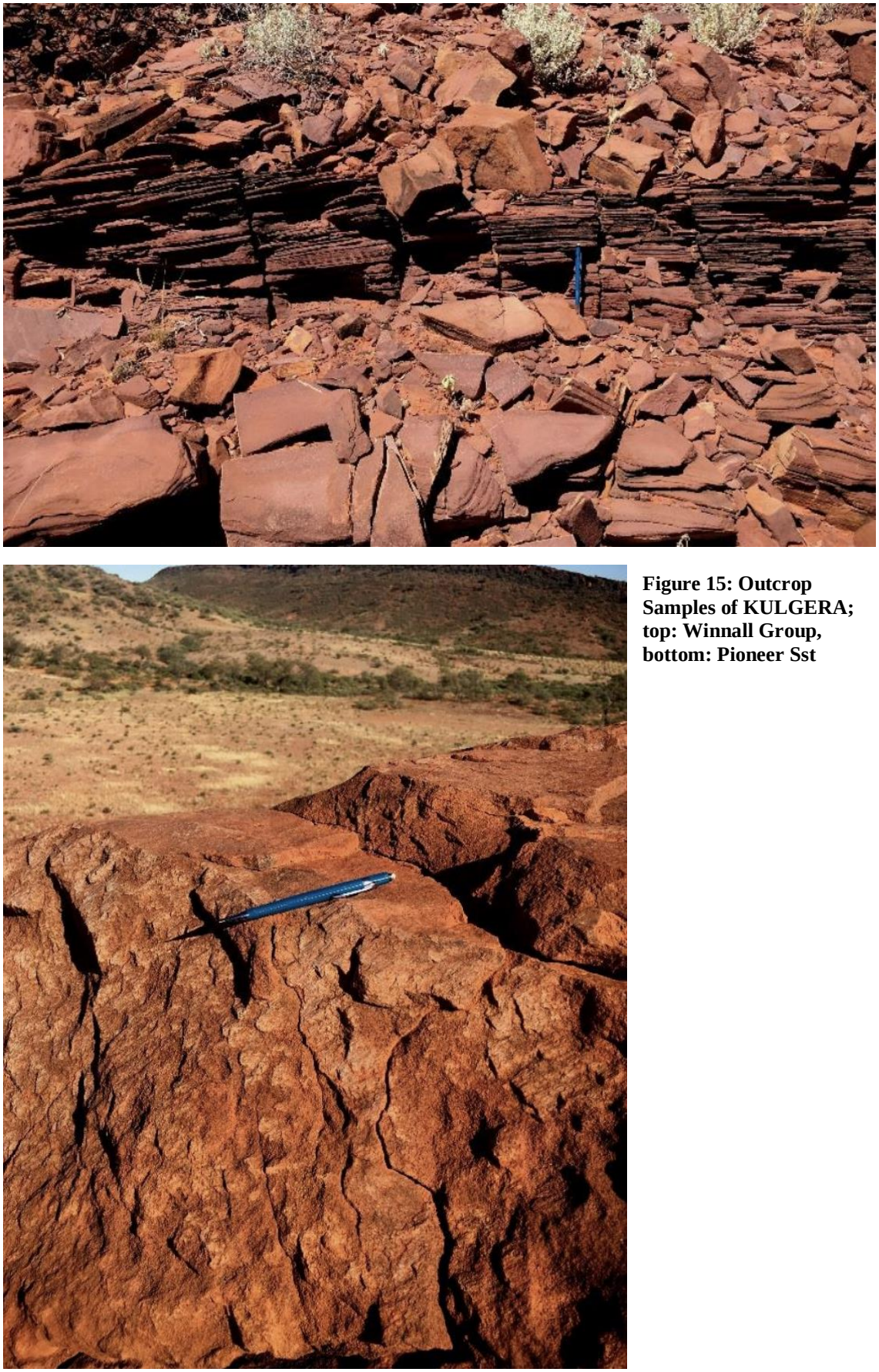

Figure 15: Outcrop Samples of KULGERA; top: Winnall Group, bottom: Pioneer Sst

APPENDIX B: EXTENDED METHODS

Mineral Separation

Crushing

1. Cut the rocks using the rock saw.
2. Make sure that the rocks are dry, clean and fresh. Ensuring that there is no lichen left on the rocks.
3. Clean the jaw crusher before and after use

a. This is done using compressed air and ethanol.

4. Line the tray with butcher paper to ensure that the samples are not contaminated.
5. The disc mill is used to achieve the zircon fraction. Clean the machine using compressed air and ethanol.
6. Move the discs until the desired gap is reached. Start at 1mm.
7. Run this through the sieve using <79 μm and >479 μm mesh. Place the sieve into the Endcotts EPL2000 Super Shaker and allow for the fractions to separate.
8. Take the course fraction >479 μm and run it through the disc mill again, changing the spacing between the discs to 0.7mm.
9. Repeat this process again with the spacing at 0.4mm.
10. Put each fraction into the sample bags. Labelling '>479 μm', 'Zircon fraction' and '<79 μm'
11. If samples are undergoing geochemistry, after they have been through the jaw crusher they are placed into the ring mill using the tungsten carbide. The ring mill is cleaned with compressed air and ethanol.
12. Quartz blank is first used to ensure contamination is kept at a minimum. The quartz is run for 1.5 minutes.
13. The samples are then placed into the tungsten carbide mill and run for 3 minutes.
14. This fraction is then placed in a sample bag for later requirements.

Separating zircons from the 'zircon fraction'

The separation was done in the Mawson Building lab B29 at Adelaide University. Before each use the room is cleaned before each use. The benches are cleaned, and the room is vacuumed. The sample is panned removing the lights from the fraction. The lights are placed into a funnel with filter paper and later dried in the oven. The heavies extracted by this method are the placed on the hotplate to dry at 50 °C. To separate the magnetic material the sample is put through the FRANTZ Magnetic Separator. Initially, the sample is run through at 1.0 amps. This will separate the highly magnetic minerals. This is repeated. The magnet is turned up to 1.6 amps. Each magnetic fraction is placed in a sample bag and clearly labelled.

Laboratory Processing

Apatite samples were prepared using conventional methods for fission track and U-Pb laser-ablation analysis (e.g. Glorie et al., 2017). Cuttings and core were crushed and panned before being magnetically separated with a Franz system. The non-magnetic fraction was further processed with heavy liquids (lithium heteropolytungstates heavy liquid and methyl iodide) to recover the apatite fraction. Individual apatite grains were picked onto double sided tape in rasters of 100-150 grains (depending on grain availability) and positioned such that the grain c-axis was parallel to the surface of the tape. Grains were mounted in an EpoxyCure resin prepared with 5g epoxy resin and 1.15g epoxy hardener. Resin was poured on the tape to cover the raster of grains, and a glass microscope slide placed over the resin such that the resin would adhere to it. Resin was allowed to set for 24 hours before the tape was removed, leaving grains embedded in the resin mount. To expose apatite grains the top of the resin mount was carefully grinded using #2000 silicon carbide paper. The mounts were subsequently polished on an Autopolisher system using 3μm and 1μm diamond suspension solutions to provide smooth surface for fission track counting. Once sufficiently polished, samples were etched to reveal fission tracks for counting. Each sample was etched in a solution of 5M nitric acid (HNO3) at 20±0.5oC for 20±0.5 seconds, then immediately washed in distilled water to remove all nitric acid and ensure etching durations were consistent between all samples.

Fission Track Counting

After etching, mounts were examined for apatite on a Zeiss AXIO Imager M2m Autoscan System, with apatite identified by the presence of etched features (scratches, fission tracks) on the grain surface. Mounts with no grains displaying these characteristics were judged not to contain any apatite, and were excluded from any further processing. Samples that contained grains with etching features but without fission tracks (so-called zero-age grains) were still processed further. Samples containing apatite were coated in a 3nm layer of gold to enhance the imaging process of the fission tracks. Apatite bearing samples were imaged using the Zeiss AXIO Imager M2m Autoscan System, and surface track densities and confined track lengths measured using FastTracks software. Fission track densities are known to be correlated with the fission track age and 238U concentration (Wagner & Van den haute, 1992). The fission track age reflects the timing of passage through the so-called apatite partial annealing zone (APAZ) at temperatures of ~60-120oC (Wagner & Van den haute, 1992).

APPENDIX C: INDIVIDUAL KDE PLOTS

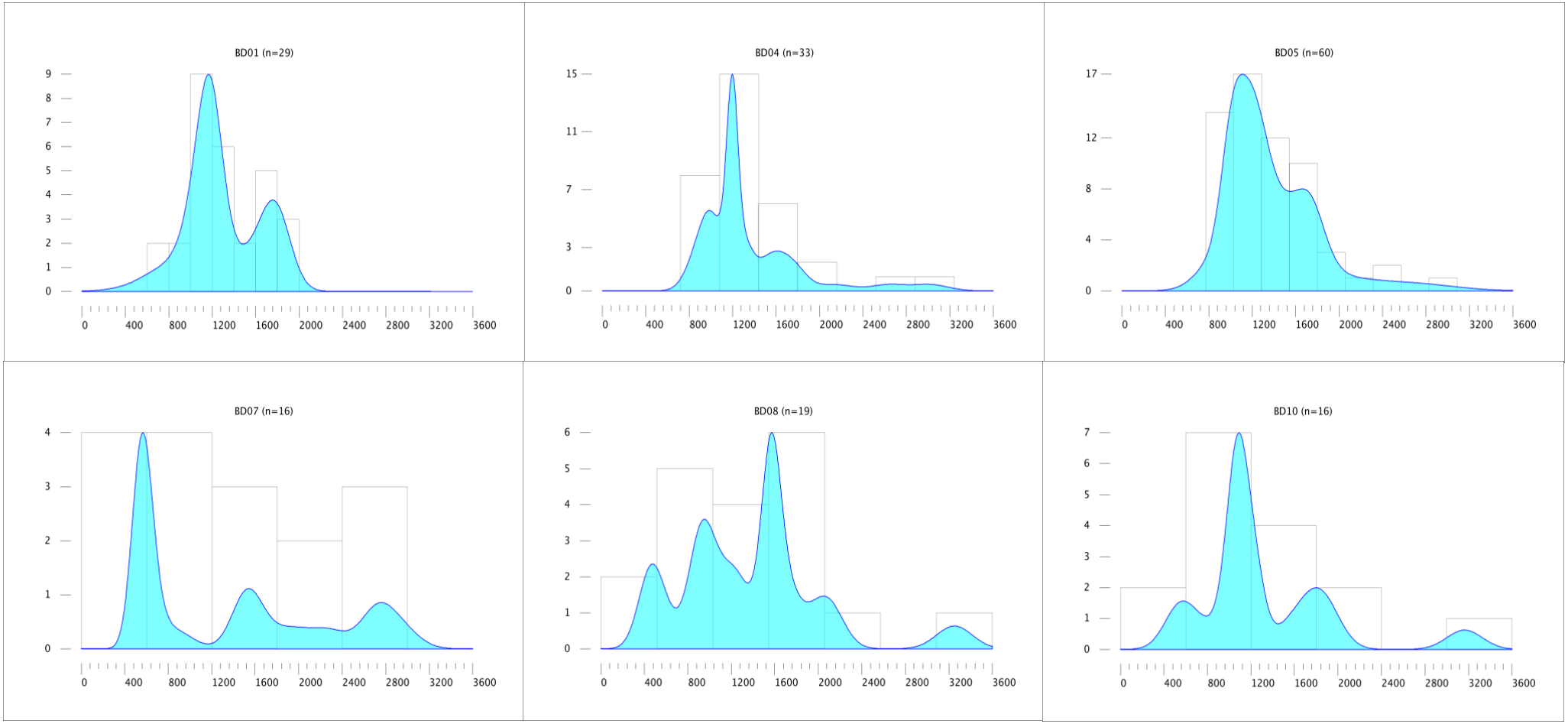

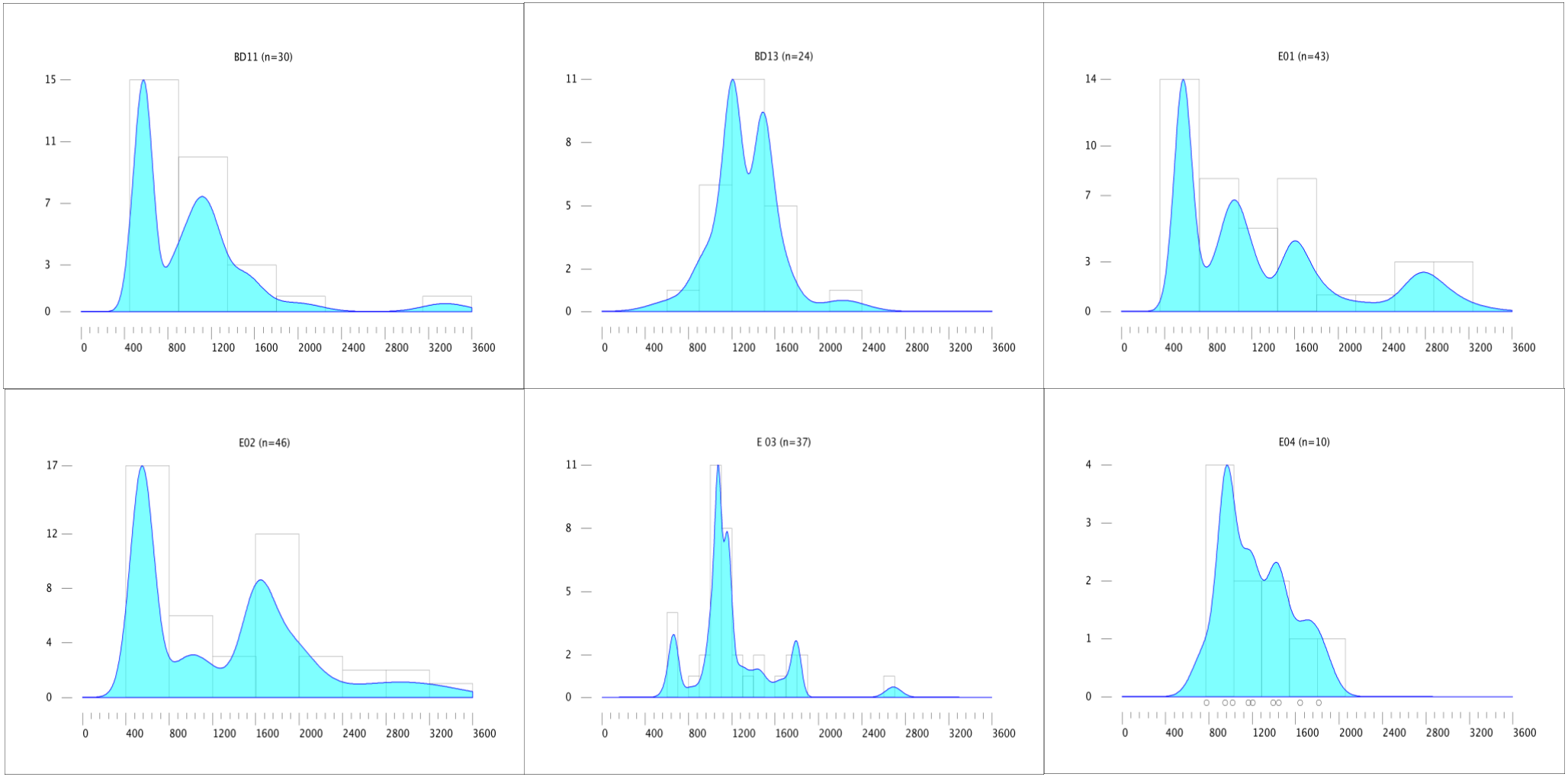
BD11 (n=30)
BD13 (n=24)
E01 (n=43)
E02 (n=46)
E 03 (n=37)
E04 (n=10)
0 400 800 1200 1600 2000 2400 2800 3200 3600

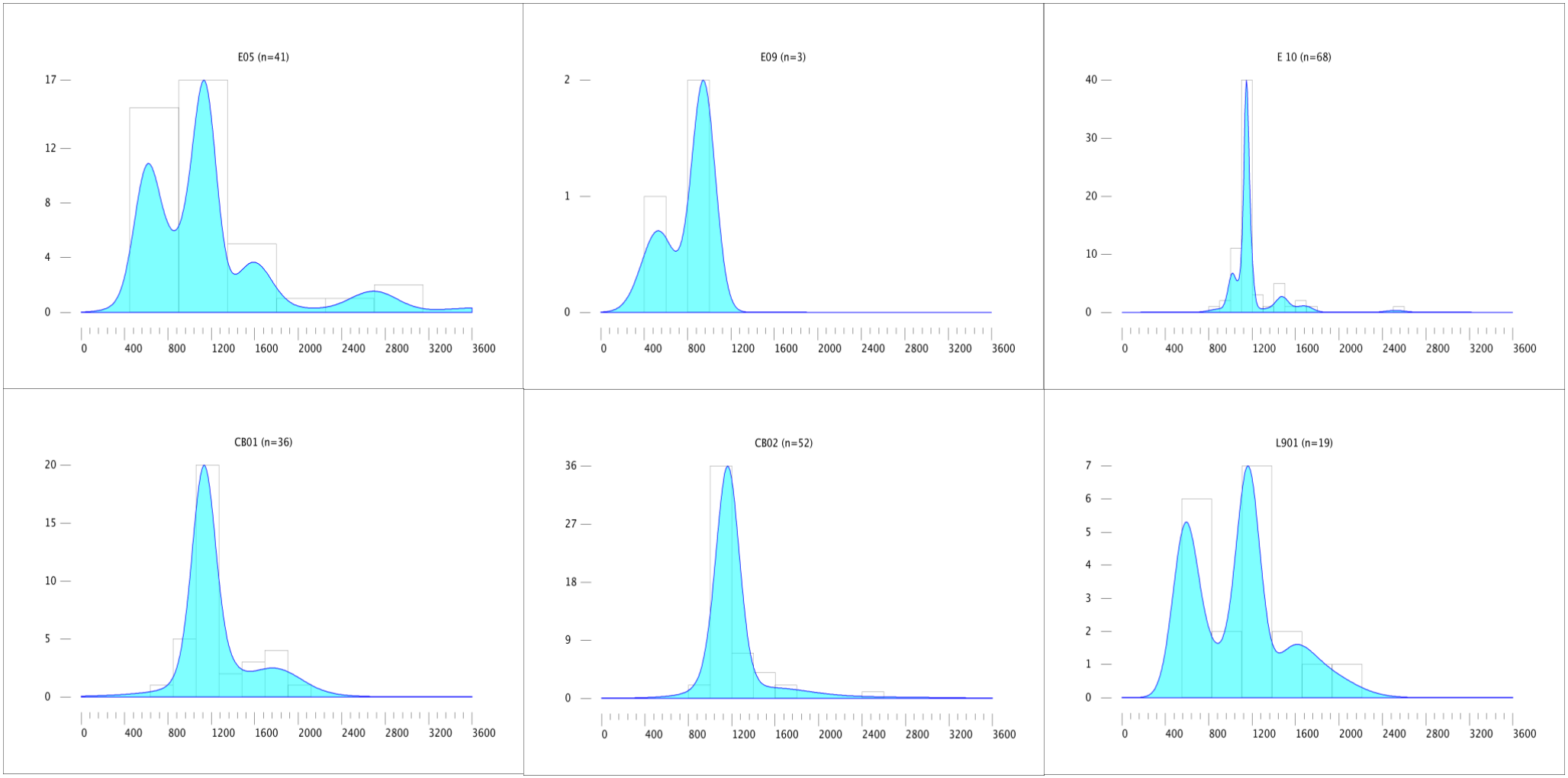
E05 (n=41)
17
12
8
4
0
0 400 800 1200 1600 2000 2400 2800 3200 3600
E09 (n=3)
2
1
0
0 400 800 1200 1600 2000 2400 2800 3200 3600
E 10 (n=68)
40
30
20
10
0
0 400 800 1200 1600 2000 2400 2800 3200 3600
CB01 (n=36)
20
15
10
5
0
0 400 800 1200 1600 2000 2400 2800 3200 3600
CB02 (n=52)
36
27
18
9
0
0 400 800 1200 1600 2000 2400 2800 3200 3600
L901 (n=19)
7
6
5
4
3
2
1
0
0 400 800 1200 1600 2000 2400 2800 3200 3600

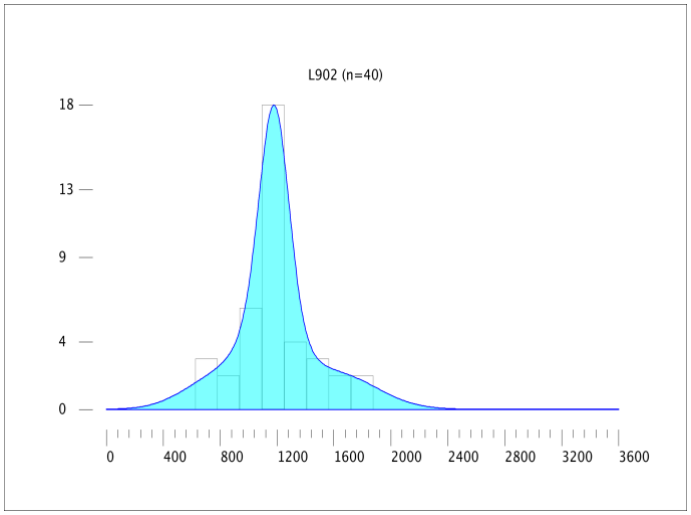
L902 (n=40)
18
13
9
4
0
0
400
800
1200
1600
2000
2400
2800
3200
3600

APPENDIX D: DATA TABLES

Zircon Data Table

B1	B4	B5	B7	B8	B10	B11	B13	B15	CB1	CB2	E1	E2	E3	E4	E5	E9	E10	L901	L902
635.4	817	793	507.4	455.4	513.8	501.4	662	519.5	685	925	496	480.1	623.7	779	491	529.3	874	554.3	680.4
777.1	848	834	519.4	460.3	593.2	505	931.4	566.4	908	980	519	495.3	657	948.7	573.1	943.6	942	561.1	692
813.2	891.3	851	525	583	845	510.7	966	574.7	994	1040	523.4	536.3	667.3	951.3	586.7	949	996	577.4	764.9
999	930	861	573	882	1003	511.3	1012.6	893	1048	1046.1	548.8	538	676	1018	590		1001	595.1	807
1006	967	948	609.2	898	1020	537	1124	917.6	1049.1	1074	549.6	541.8	830	1165	590.6		1006	603.6	823.6
1031.4	984	988	610	979	1061	571.1	1210	1015	1052	1077	559.5	543	967.4	1203	602.8		1011	688.3	976
1063.4	1004	990	664	1022	1098	591	1175	1067.6	1080	1091	573	545.2	977	1445	608.4		1013	841	995
1105.6	1041	1000	857.9	1187	1102	608.5	1154	1072	1081	1094	573.1	547.2	1017	1392	611.9		1026	928.9	998
1113	1095	1003	1470	1236	1173	609.8	1211	1083	1082	1098	579.2	548.6	1025.6	1642	623.3		1028	1111	1046
1127	1099	1004	1537	1542	1223	611	1262	1098	1103	1105	583.4	548.8	1026	1813	689.7		1033	1132	1071
1138	1174	1005	1635	1388	1237	618.8	1213	1099	1119	1106	604.9	550	1051		696		1058	1151	1083
1162	1174	1006	1942	1545	1558	620	1233	1110	1119	1113	607.2	554.8	1070.1		725		1072	1158	1123
1198	1195	1015	2278	1590	1723	853	1313	1114	1123	1127	608.6	558	1071		874		1091	1191	1131
1209	1195	1015	2770	1580	1831	867	1464	1126	1130	1135	678.2	569.3	1073		883		1095	1197	1139
1209	1196	1061	2674	1679	1935	875	1500	1128	1130	1142	788	580	1074		891.9		1103	1205	1144
1223	1199	1085	2950	1758	3165	1001	1476	1141	1142	1143	883	585	1081.1		969		1108	1554	1158
1241	1199	1085		2026		1022	1480	1164	1146	1144	904	588.7	1091		993		1116	1751	1173
1276	1207	1095		2114		1035.6	1384	1169	1147	1147	967	930.2	1097		1023		1125	1580	1175
1286	1217	1143		3252		1101	1479	1616	1156	1151	981	993.2	1132		1047.8		1125	1961	1177
1439	1328	1144				1124	1543	1615	1167	1155	1011	1001.2	1139		1102		1126		1178
1401	1220	1145				1148	1657	1626	1169	1158	1033	1024	1142		1109		1128		1180
1600	1308	1145				1218	1604	1739	1169	1161	1073	1038	1161		1110		1128		1181

1707	1447	1157				1233	1713	1815	1176	1161	1083	1145	1168		1113		1128		1191
1658	1303	1188				1261	2226	1870	1180	1162	1122	1443	1171		1132		1130		1198
1814	1503	1191				1483		2748	1256	1167	1197	1641	1184		1152		1134		1206
1730	1626	1192				1340		3340	1265	1173	1204	1586	1195		1153		1135.3		1212
1788	1565	1228				1618			1274	1174	1213	1626	1258		1158		1141		1230
1807	1684	1234				1522			1278	1174	1445	1620	1290		1163		1141		1237
1840	1767	1251				2008			1519	1177	1595	1586	1334		1163		1145		1241
	1806	1267				3357			1551	1177	1569	1610	1546		1189		1146		1255
	2144	1283							1659	1178	1572	1606	1478		1193		1146		1293
	2637	1300							1758	1182.8	1573	1612	1625		1194		1147		1300
	3022	1315							1850	1183	1682	1677	1788		1539		1148		1349
		1317							1785	1185	1777	1802	1801		1604		1148		1350
		1344							1981	1185.3	1792	1903	1707		1619		1148		1409
		1325							1867	1189	2002	1811	1800		1570		1152		1482
		1460								1191	2301	1906	2691		1592		1153		1703
		1442								1194.5	2705	1916			1828		1153		1683
		1494								1204	2780	2045			2713		1154		1772
		1346								1218	2714	2006			2641		1155		1824
		1469								1219.4	2961	2090			2719		1155		
		1520								1232	2897	2571			3697		1157		
		1486								1235	3148	2715					1158		
		1740								1248		2881					1169		
		1657								1249		3176					1170		
		1638								1513		3288					1170		
		1589								1464							1172		
		1840								1584							1174		
		1570								1547							1176		

		1828								1699							1179		
		1728								1741							1187		
		1745								2548							1191		
		1713															1191		
		1780															1195		
		1743															1201		
		2062															1205		
		2014															1261		
		2382															1449		
		2562															1353		
		2879															1440		
																	1485		
																	1477		
																	1498		
																	1561		
																	1710		
																	1609		
																	1694		
																	2520		

Mereenie Sst	Carmichael Sst	Stairway Sst	Mt Currie Conglomerate	Winnall Group	Pioneer Sst
554.3	455.4	480.1	685	491	623.7
561.1	460.3	495.3	908	573.1	657
577.4	583	496	994	586.7	667.3
595.1	635.4	501.4	1048	590	676
603.6	662	505	1049.1	590.6	830
688.3	680.4	507.4	1052	602.8	967.4
841	692	510.7	1080	608.4	977
928.9	764.9	511.3	1081	611.9	1017
1111	777.1	513.8	1082	623.3	1025.6
1132	807	519	1103	689.7	1026
1151	813.2	519.4	1119	696	1051
1158	823.6	523.4	1119	725	1070.1
1191	882	525	1123	779	1071
1197	898	529.3	1130	793	1073
1205	925	536.3	1130	834	1074
1554	931.4	537	1142	851	1081.1
1751	966	538	1146	861	1091
1580	976	541.8	1147	874	1097
1961	979	543	1156	883	1132
	980	545.2	1167	891.9	1139
	995	547.2	1169	948	1142
	998	548.6	1169	948.7	1161
	999	548.8	1176	951.3	1168
	1006	548.8	1180	969	1171
	1012.6	549.6	1256	988	1184

	1022	550	1265	990	1195
	1031.4	554.8	1274	993	1258
	1040	558	1278	1000	1290
	1046	559.5	1519	1003	1334
	1046.1	569.3	1551	1004	1478
	1063.4	571.1	1659	1005	1546
	1071	573	1758	1006	1625
	1074	573	1785	1015	1707
	1077	573.1	1850	1015	1788
	1083	579.2	1867	1018	1800
	1091	580	1981	1023	1801
	1094	583.4		1047.8	2691
	1098	585		1061	
	1105	588.7		1085	
	1105.6	591		1085	
	1106	593.2		1095	
	1113	604.9		1102	
	1113	607.2		1109	
	1123	608.5		1110	
	1124	608.6		1113	
	1127	609.2		1132	
	1127	609.8		1143	
	1131	610		1144	
	1135	611		1145	
	1138	618.8		1145	
	1139	620		1152	
	1142	664		1153	

	1143	678.2		1157	
	1144	788		1158	
	1144	817		1163	
	1147	845		1163	
	1151	848		1165	
	1154	853		1188	
	1155	857.9		1189	
	1158	867		1191	
	1158	874		1192	
	1161	875		1193	
	1161	883		1194	
	1162	891.3		1203	
	1162	904		1228	
	1167	930		1234	
	1173	930.2		1251	
	1173	942		1267	
	1174	943.6		1283	
	1174	949		1300	
	1175	967		1315	
	1175	967		1317	
	1177	981		1325	
	1177	984		1344	
	1177	993.2		1346	
	1178	996		1392	
	1178	1001		1442	
	1180	1001		1445	
	1181	1001.2		1460	

	1182.8	1003		1469	
	1183	1004		1486	
	1185	1006		1494	
	1185.3	1011		1520	
	1187	1011		1539	
	1189	1013		1570	
	1191	1020		1570	
	1191	1022		1589	
	1194.5	1024		1592	
	1198	1026		1604	
	1198	1028		1619	
	1204	1033		1638	
	1206	1033		1642	
	1209	1035.6		1657	
	1209	1038		1713	
	1210	1041		1728	
	1211	1058		1740	
	1212	1061		1743	
	1213	1072		1745	
	1218	1073		1780	
	1219.4	1083		1813	
	1223	1091		1828	
	1230	1095		1828	
	1232	1095		1840	
	1233	1098		2014	
	1235	1099		2062	
	1236	1101		2382	

	1237	1102		2562	
	1241	1103		2641	
	1241	1108		2713	
	1248	1116		2719	
	1249	1122		2879	
	1255	1124		3697	
	1262	1125			
	1276	1125			
	1286	1126			
	1293	1128			
	1300	1128			
	1313	1128			
	1349	1130			
	1350	1134			
	1384	1135.3			
	1388	1141			
	1401	1141			
	1409	1145			
	1439	1145			
	1464	1146			
	1464	1146			
	1476	1147			
	1479	1148			
	1480	1148			
	1482	1148			
	1500	1148			
	1513	1152			

	1542	1153			
	1543	1153			
	1545	1154			
	1547	1155			
	1580	1155			
	1584	1157			
	1590	1158			
	1600	1169			
	1604	1170			
	1657	1170			
	1658	1172			
	1679	1173			
	1683	1174			
	1699	1174			
	1703	1174			
	1707	1176			
	1713	1179			
	1730	1187			
	1741	1191			
	1758	1191			
	1772	1195			
	1788	1195			
	1807	1195			
	1814	1196			
	1824	1197			
	1840	1199			
	2026	1199			

	2114	1201			
	2226	1204			
	2548	1205			
	3252	1207			
		1213			
		1217			
		1218			
		1220			
		1223			
		1233			
		1237			
		1261			
		1261			
		1303			
		1308			
		1328			
		1340			
		1353			
		1440			
		1443			
		1445			
		1447			
		1449			
		1470			
		1477			
		1483			
		1485			

		1498			
		1503			
		1522			
		1537			
		1558			
		1561			
		1565			
		1569			
		1572			
		1573			
		1586			
		1586			
		1595			
		1606			
		1609			
		1610			
		1612			
		1618			
		1620			
		1626			
		1626			
		1635			
		1641			
		1677			
		1682			
		1684			
		1694			

		1710			
		1723			
		1767			
		1777			
		1792			
		1802			
		1806			
		1811			
		1831			
		1903			
		1906			
		1916			
		1935			
		1942			
		2002			
		2006			
		2008			
		2045			
		2090			
		2144			
		2278			
		2301			
		2520			
		2571			
		2637			
		2674			
		2705			

		2714			
		2715			
		2770			
		2780			
		2881			
		2897			
		2950			
		2961			
		3022			
		3148			
		3165			
		3176			
		3288			
		3357			

Apatite Data Table

	238/206	s[8/6]	207/206	s[7/6]	t (Ma)	SD t (Ma)
B3(i)-2.d	3.03030303	0.006	0.207	0.008	142.691411	22.31
B3(ii)-4.d	4.45831476	0.00385	0.1453	0.00255	114.084288	14.25
B3(ii)-7.d	3.50877193	0.0055	0.399	0.0065	174.537935	20.12
B3(ii)-8.d	3.58422939	0.0055	0.383	0.0065	180.63161	24.3
B12(ii)-5.d	0.1912	0.00395	0.417	0.0085	228.295344	22.9
B12(ii)-9.d	0.266	0.005	0.323	0.0065	333.5	41.18
B12(ii)-10.d	0.2233	0.0035	0.2141	0.003	85.7349218	15.46
B12(ii)-11.d	1.025	0.025	0.863	0.0135	2278.45054	351.39
B12(i)-16.d	0.472	0.017	0.659	0.021	304.049057	99.25

Name	238U Dur	SD	RF	Ns	A (unadjusted)	A	rho s	t (Ma)	SD t	t (Ma)	SD t
B3(i)-2.d	48.800	3.1	6.35245902	49	1.38E-05	1382	3545586.11	143.80	22.48	0	0.00
B3(ii)-4.d	152.700	8.9	5.82842174	82	9.27E-06	9.27E+02	8.85E+06	114.98	14.36	0	0.00
B3(ii)-7.d	25.800	1.3	5.03875969	93	4.05E-05	4.05E+03	2.30E+06	175.89	20.28	0	0.00
B3(ii)-8.d	25.000	1.5	6	69	2.99E-05	2.99E+03	2.31E+06	182.04	24.49	0	0.00
B12(ii)-5.d	32.500	1.8	5.53846154	143	3.76E-05	3760	3803191.49	230.06	23.08	0	0.00
B12(ii)-9.d	42.400	3.1	7.31132075		1.38E-05	1382	0	0.00	#DIV/0!	333.5	41.18
B12(ii)-10.d	106.000	11	10.3773585	46	9.99E-06	998.5	4606910.37	86.41	15.58	0	0.00
B12(ii)-11.d	3.260	0.22	6.74846626	52	1.16E-05	1159	4486626.4	2293.56	353.72	0	0.00
B12(i)-16.d	1.730	0.14	8.09248555	10	3.69E-05	3687	271223.217	306.39	100.01	0	0.00